การปรับปรุงประสิทธิภาพของเซลล์แสงอาทิตย์ชนิดสีย้อมไวแสงที่มี TiO_2 อิเล็กโทรดแบบพ่นเคลือบดัดแปรด้วย CuO, NiO หรือ In_2O_3

นายสกรรณ์ ปรีดาวิจิตรกุล

วิทยานิพนธ์นี้เป็นส่วนหนึ่งของการศึกษาตามหลักสูตรปริญญาวิศวกรรมศาสตรมหาบัณฑิต
สาขาวิชาวิศวกรรมเคมี ภาควิชาวิศวกรรมเคมี
คณะวิศวกรรมศาสตร์ จุฬาลงกรณ์มหาวิทยาลัย
ปีการศึกษา 2560

IMPROVING THE EFFICIENCY OF DYE-SENSITIZED SOLAR CELLS WITH SPRAY-COATED TiO_2 ELECTRODE MODIFIED BY CuO, NiO, OR In_2O_3

Mr. Sakun Preedavijitkul

A Thesis Submitted in Partial Fulfillment of the Requirements
for the Degree of Master of Engineering Program in Chemical Engineering
Department of Chemical Engineering
Faculty of Engineering
Chulalongkorn University
Academic Year 2017

Thesis Title	IMPROVING THE EFFICIENCY OF DYE-SENSITIZED SOLAR CELLS WITH SPRAY-COATED TiO_2 ELECTRODE MODIFIED BY CuO, NiO, OR In_2O_3
By	Mr. Sakun Preedavijitkul
Field of Study	Chemical Engineering
Thesis Advisor	Akawat Sirisuk, Ph.D.

Accepted by the Faculty of Engineering, Chulalongkorn University in Partial Fulfillment of the Requirements for the Master's Degree

.....Dean of the Faculty of Engineering

(Associate Professor Supot Teachavorasinskun, D.Eng.)

THESIS COMMITTEE

.....Chairman

(Professor Siriporn Damrongsakkul, Ph.D.)

.....Thesis Advisor

(Akawat Sirisuk, Ph.D.)

.....Examiner

(Chalida Klaysom, Ph.D.)

.....External Examiner

(Assistant Professor Tanawan Pinnarat, Ph.D.)

สกรรณ์ ปรีดาวิจิตรกุล : การปรับปรุงประสิทธิภาพของเซลล์แสงอาทิตย์ชนิดสีย้อมไวแสงที่มี TiO_2 อิเล็กโทรดแบบพ่นเคลือบดัดแปรด้วย CuO, NiO หรือ In_2O_3 (IMPROVING THE EFFICIENCY OF DYE-SENSITIZED SOLAR CELLS WITH SPRAY-COATED TiO2 ELECTRODE MODIFIED BY CuO, NiO, OR In_2O_3) อ.ที่ปรึกษาวิทยานิพนธ์หลัก: ดร. อัครวัต ศิริสุข, 83 หน้า.

งานวิจัยนี้ได้ทำการศึกษาพิจารณาการเติม คอปเปอร์ออกไซด์, นิกเกิลออกไซด์ หรือ อินเดียมออกไซด์ ลงบนไททาเนียมไดออกไซด์ ที่ใช้เป็นอิเล็กโทรดสำหรับเซลล์แสงอาทิตย์ชนิดสีย้อมไวแสง ถูกสังเคราะห์ขึ้นด้วยวิธีโซล-เจล และทำการพ่นเคลือบลงบนกระจกโปร่งแสงนำไฟฟ้า FTO ด้วยเครื่องพ่นเคลือบอัลตร้าโซนิค จำนวน 500 รอบ จากนั้นนำไปเผาที่อุณหภูมิ 400 องศาเซลเซียส เป็นเวลาสองชั่วโมง โดยปริมาณการเติมแต่งโลหะออกไซด์ออกไซด์ อยู่ในช่วงร้อยละ 0, 0.1, 0.5, 1.0 และ 3.0 โดยน้ำหนัก สำหรับประสิทธิภาพของเซลล์แสงอาทิตย์ชนิดสีย้อมไวแสงแบบที่ใช้ไททาเนียมไดออกไซด์เป็นอิเล็กโทรด มีประสิทธิภาพของเซลล์อยู่ที่ 3.40±0.62% การเติมคอปเปอร์ออกไซด์ที่ร้อยละ 0.1, นิกเกิลออกไซด์ที่ร้อยละ 0.5 และอินเดียมออกไซด์ที่ร้อยละ 1.0 ลงบนไททาเนียมไดออกไซด์ ทำให้ประสิทธิภาพของเซลล์เพิ่มขึ้นเป็น 4.03±0.58%, 5.17±0.07% และ 6.21±0.87% ตามลำดับ การเพิ่มขึ้นของพื้นที่ผิวจำเพาะของขั้วอิเล็กโทรด ทำให้ปริมาณการดูดซับสีย้อมรูทีเนียมชนิด N3 บนขั้วอิเล็กโทรดมีมากขึ้น ส่งผลให้มีการเพิ่มขึ้นของกระแสลัดวงจร ทำให้ประสิทธิภาพของเซลล์แสงอาทิตย์เพิ่มขึ้นของชั้นฟิล์มอิเล็กโทรดแบบชั้นเดียว จากนั้นทำการศึกษาผลของชั้นฟิล์มอิเล็กโทรดแบบสองชั้น โดยใช้ชั้นไททาเนียมไดออกไซด์บริสุทธิ์ ร่วมกับชั้นอินเดียมออกไซด์ที่ร้อยละ 1.0 พบว่าเกิดการกระเจิงของแสงภายในอุปกรณ์เกิดขึ้นดีกว่าแบบชั้นเดียว ทำให้ประสิทธิภาพของเซลล์เพิ่มขึ้นจาก 6.21±0.87% เป็น 7.95±0.40% เมื่อเปรียบเทียบกับชั้นอิเล็กโทรดแบบชั้นเดียว

ภาควิชา วิศวกรรมเคมี ลายมือชื่อนิสิต .....

สาขาวิชา วิศวกรรมเคมี ลายมือชื่อ อ.ที่ปรึกษาหลัก .....

ปีการศึกษา 2560

5970332021 : MAJOR CHEMICAL ENGINEERING

KEYWORDS: DYE-SENSITIZED SOLAR CELL / TITANIUM DIOXIDE / ULTRASONIC SPRA
COATING / COPPER OXIDE / NICKEL OXIDE / INDIUM OXIDE

SAKUN PREEDAVIJITKUL: IMPROVING THE EFFICIENCY OF DYE-SENSITIZE
SOLAR CELLS WITH SPRAY-COATED TiO_2 ELECTRODE MODIFIED BY CuO, NiC
OR In_2O_3. ADVISOR: AKAWAT SIRISUK, Ph.D., 83 pp.

This research investigated the application of the CuO/TiO_2, NiO/TiO_2, c In_2O_3/TiO_2 thin film electrode in dye-sensitized solar cells (DSSCs). Second metal oxid and TiO_2 sols were synthesized separately via sol-gel methods. The sols were mixe and sprayed onto the fluorine-doped tin oxide glass substrates. The amount of secon metal oxide added to TiO_2 was varied at 0, 0.1, 0.5, 1.0, and 3.0%wt. The electrod layer was sintered at 400°C for two hours. The addition of CuO, NiO, and In_2C produced the photovoltaic efficiency of the cell 4.03±0.58% with 0.1%wt. CuO/TiO 5.17±0.07% with 0.5%wt. NiO/TiO_2, and 6.21±0.87% with 1.0%wt. In_2O_3/TiO respectively. The DSSCs with 1.0%wt. In_2O_3/TiO_2 electrode coated with N3 dy possessed the highest power conversion efficiency, compared with that of DSSCs wit pure TiO_2 (3.40±0.62%) electrode coated with the same dye. The DSSCs with single layered NiO/TiO_2 or In_2O_3/TiO_2 electrode had the high value of short-circuit currer density (J_{sc}) and consequently high efficiency, which is due to the larger specific surfac area of the electrode available for dye adsorption. Furthermore, the double-layere electrode structure with pure TiO_2 as the under-layer and 1.0%wt. In_2O_3/TiO_2 as th over-layer was studied. The cell efficiency was increased from 6.21±0.87% t 7.95±0.40%, compared to the single-layered 1.0%wt. In_2O_3/TiO_2 electrode. This can b attributed to light scattering effect as a result of mismatched particle size in the tw layers, which increased the reflection of light back into the cell. The enhancement c light reflection was evident from the result of UV-Visible diffuse reflectanc spectroscopy.

Department:	Chemical Engineering	Student's Signature	.....
Field of Study:	Chemical Engineering	Advisor's Signature	.....
Academic Year:	2017		

ACKNOWLEDGEMENTS

I would first like to thank my thesis advisor Dr. Akawat Sirisuk of the Center of Excellence on Catalysis and Catalytic Reaction Engineering, Faculty of Engineering, Chulalongkorn University. The door to my office was always opened whenever I ran into a trouble spot or had a question about my research or writing. He consistently allowed this research to be my own work, but steered me in the right the direction when he thought I needed it.

I would also like to thank the Polymers for Energy Environment and Technology Research & Development Group (PENTEC), KMUTT for the I-V characteristic measurement.

I would also like to acknowledge Professor Dr. Siriporn Damrongsakkul and Dr. Chalida Klaysom of the Department of Chemical Engineering at Chulalongkorn University, and Assistant Professor Dr. Tanawan Pinnarat of the Department of Chemical Engineering at King Mongkut's Institute of Technology Ladkrabang as my thesis committee. I am gratefully indebted to them for their very valuable comments on this thesis.

Finally, I must express my very profound gratitude to my parents and to my family for providing me with unfailing support and continuous encouragement throughout my years of study and through the process of researching and writing this thesis. This accomplishment would not have been possible without them. Thank you.

CONTENTS

Page

Page

Page

LIST OF TABLES

LIST OF FIGUERS

CHAPTER 1
INTRODUCTION

1.1 Rationale

Electrical energy is an important factor for the development of the country. Its source can be either renewable or non-renewable. Renewable energy is the energy created from renewable sources such as sunlight, geothermal heat, and others. Solar cells are photovoltaic all that convert the energy of the sunlight into electricity.

Dye-sensitized solar cells (DSSCs), the third generation solar cells, has gained attention because of their inexpensive production, highly efficient conversion of solar energy into electricity, and simple manufacturing processes. DSSC possesses conversion efficiency that is comparable to that of amorphous Si-based solar cells [1-3]. In 1991, O'Regan and Grätzel reported that a DSSC, which is based on TiO_2 nanoparticle, has high photovoltaic conversion efficiency so this type of solar cell has attracted much commercial interest [4].

DSSC typically consists of a semiconductor (TiO_2, ZnO, and others) thin film - served as a photoanode electrode - that is coated on fluorine-doped tin oxide (FTO) glass; a dye sensitizer (e.g. ruthenium-based dye N719 or N3); an electrolyte (I_3^-/I^- redox couples) injected between dye sensitizer and counter electrode; and a counter electrode (platinum and graphite) deposited on FTO glass. When the dye is excited by sunlight, it rapidly injects an electron into photoanode electrode. Electrons are subsequently injected into the conduction band of the semiconductor and quickly shuttled to the external circuit through the conductive glass, producing an electric current. The electrolyte can restore the dye to its original state by electron donation. [5-7]

Several attempt have been made to increase the conversion efficiency of dye-sensitized solar cells such as modifying the properties of TiO_2 electrode by adding

another metal oxide [8] into the lattice of TiO_2 to increase surface area; using pre-coated with passivation layer of another high band gap of metal oxide to prevent the electron recombination; fabricating a double-layered structure as a light scattering layer to boost the light harvesting. Moreover, there have been other approaches to increase the efficiency conversion by developing a new dye-sensitizer for absorption in broad wavelength of light or resolving the leakage problems of volatile electrolyte that exhibited remarkable efficiency and stability.

In this research, we focused mainly on the improvement of the photovoltaic conversion efficiency of DSSC by adding another metal oxide, namely, CuO, NiO, or In_2O_3 to TiO_2 for use as thin film electrode layer because the second metal oxide have been investigated for photovoltaic, proton reduction applications, and high natural abundance on the earth crust. In the visible range that sensitizers for DSSC must exhibit the high extinction coefficient and absorption bands located in the lower energy part of the spectrum to be exploitable. The double-layered structure was also investigated to improve on a light scattering inside for cell and increase light absorption.

1.2 Objectives

1. To enhance the efficiency of dye-sensitized solar cells with TiO_2 electrode modified by adding CuO, NiO, or In_2O_3 into electrode layer.

2. To improve the efficiency of a dye-sensitized solar cells by using double-layered structure consisting an over- and under-layer film electrode.

1.3 Research scopes

1.3.1 Part I

- Titanium dioxide (TiO_2) and the second metal oxide (CuO, NiO, and In_2O_3) were prepared by sol-gel methods.
- The amount of CuO, NiO, and In_2O_3 that were added to TiO_2 ranged from 0 to 3%wt.
- Transparent electrode was characterized by several techniques.

- X-ray diffraction
- Nitrogen physisorption
- UV-visible diffuse reflectance spectroscopy
- Inductively couple plasma optical emission spectroscopy

- The efficiency of dye-sensitized solar cell was measured by IV-tester.

1.3.2 Part II

- Fabricate a DSSC with a double-layered thin film electrode with one layer being the electrode that produced the highest efficiency from Part I.
- Characterize the double-layered electrode by several techniques mentioned in Part I.

This thesis is arranged as follow:

Chapter 1 presented the introduction and objectives of this study.

Chapter 2 presented the theory of dye-sensitized solar cell, including the components and operation principles of dye-sensitized solar cell.

Chapter 3 presented the literature reviews of previous works related to this research.

Chapter 4 presented the synthesis of TiO_2 and modified TiO_2 electrodes by sol gel methods, fabrication of dye-sensitized solar cells, and characterization techniques used in this study.

Chapter 5 presented experimental details and characterization in the results and discussion section.

Chapter 6 presented conclusions and recommendations for future research.

CHAPTER 2
THEORY

Dye sensitized solar cells (DSSCs)

Dye-sensitized solar cells are an efficient type of thin-film photovoltaic cell. Most of the materials used are low-cost. However, a handful of more costly materials are necessary, such as ruthenium and platinum. They were Grätzel and O'Regan in 1991 who first introduced an attractive and low-cost solar cell namely dye-sensitized solar cell which based on the TiO_2 material [4]. DSSC is consisted of a cathode of conductive glass coated with Platinum and a photoanode of conductive glass coated with TiO_2 film, on a photoanode substrate contained a monolayer of ruthenium dyes and an electrolyte of certain organic solvent containing a redox couple, such as I^- and I_3^-. [9]

2.1 Components of DSSCs

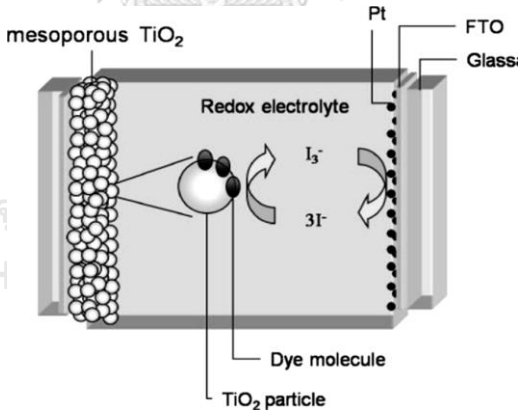

Figure 2.1 Schematic overview of a dye-sensitized solar cell [6]

2.1.1 Titanium dioxide or Titania (TiO_2) electrode

In DSSC, titanium dioxide (TiO_2) is one of the most promising materials used for nanoporous thin film due to its appropriate energy levels, dye adsorption ability, low cost, easy preparation, and high power conversion efficiency. TiO_2-based DSSCs has shown that the light harvesting efficiency of TiO_2 was influenced by its crystalline phase, particle size, surface area, dye affinity, and film porosity. [10, 11]

TiO_2 is a semiconductor having three polymorphisms including tetragonal rutile, tetragonal anatase and orthorhombic brookite. Rutile structure is the most thermodynamically stable phase, while the other two are metastable. [12] TiO_2 of anatase phase has wider energy band gap of 3.2 eV compared to the rutile phase which has 3.0 eV, and hence it has better photo-activity performance and suitable for DSSC application. [13] Nanoparticles of TiO_2 occur in three forms anatase, rutile, and brookite. Anatase is metastable and can be easily transformed into more stable phase such a rutile phase when was heating at high temperature. The rutile phase has outstanding light-scattering characteristics due to its high refractive index [14], which is a beneficial property of effective light harvesting. However, many literatures have mentioned that the combination of anatase and rutile in proper ratio can express more effective than the pure phase owing to the electron-hole separation at the interface between phases and the formation of interband gap trap which may influence interparticle carrier transportation. [11]

There are several methods that can be used to synthesize anatase TiO_2. In general, the method that have been reported for anatase synthesis are sol-gel, solvothermal, chemical vapor deposition, and precipitation method. [15, 16] The different method can give the difference of surface area, pore size, morphologies, and phase of TiO_2. Compare to the other techniques, a sol-gel is mostly used because this method has many advantages such as a possibility of making deposition on complex-shaped substrates, easy control of doping level, simple equipment and inexpensive start-up material [17, 18]. These include that it can be prepared at room temperature, applied by using ultrasonic spray coater to aid dispersion, obtained high surface area and better thermal stability than stirring method.

A sol-gel process occurs in liquid solution of organometallic precursor (e.g., Titanium tetraisopropoxide or TTIP), which lead to the formation of sol by means of hydrolysis and polycondensation of titanium alkoxide proceeds according to the following scheme [19]:

Hydrolysis: $Ti(OR)_4 + H_2O \longrightarrow Ti(OR)_3(OH) + ROH$ (2.1)

Alcohol condensation: $Ti(OR)_4 + Ti(OR)_3(OH) \longrightarrow Ti_2O(OR)_6 + ROH$ (2.2)

The reaction stops with the inclusion of two water molecule

Water condensation: $Ti(OR)_4 + 2H_2O \longrightarrow TiO_2 + ROH$ (2.3)

A typical example of the alkoxide-type solutions without hydrolysis (or stabilization) are often preferred for obtaining TiO_2.

The sol is made of many solid particles of few hundred nanometers suspended in a liquid phase. After that, the particles coalesce into gel, in which solid macromolecules are immersed in a liquid phase. Drying the gel at low temperature produces porous solid matrices. To obtain a final product, the gel in heated. This treatment serves several purpose, i.e. to remove solvent, to decompose anion such as alkoxide or carbonates to give oxides, to rearrange of the structure of solid, and to allow crystallization to occur.

2.1.2 Counter electrode

Counter electrode (CE) is one of the most important components in DSSCs. The main task of counter electrode is that a) it acts as a catalyst by reducing the redox species which are the mediators for regenerating the sensitizer (dye) after the electron injection, or b) for collecting the hole from the hole-transporting materials in a solid state DSSC. Most of the research in DSSC are focused onto boost the short-circuit current density (J_{sc}), open-circuit voltage (V_{oc}), and fill-factor (FF) for increasing the efficiency. Normally a Pt-coated on FTO is used as a counter electrode. By improving the counter electrode material, fill-factor (FF) of the cell rises, which is mainly influenced by the series resistance of the cell which is related to the slope of the tangent line to the current density (J) - Voltage (V) curve at V_{oc}. Series resistance is a combination of Warburg impedance relative to the Nernst diffusion of I_3^- species in the electrolyte, which is the impedance related to charge transfer and recombination at

the TiO_2/dye/electrolyte interface, resistance at the fluorine-doped tin oxide (FTO) glass, and the charge-transfer resistance at the counter electrode and the electrolyte interface. [20]

2.1.3 Sensitizing dye

Dye sensitizer performs a substantial role in absorbing broad wavelength of sunlight especially in visible wavelength, numerous researches have focused on how to extend the light absorption of several organic metal complexes such as /Ru polypyridyl complexes/ are employed as change-transfer sensitizers.

Ruthenium dye DSSCs were first reported in 1991 by O'Regan and Grätzel [4]. These first ruthenium dye DSSCs achieved a 7.1% conversion efficiency (Figure 2.2). However, the structure of the ruthenium dye was complicated and contained three ruthenium metal centers. In 1993, Nazeeruzzin et al. [21] published DSSCs with 10.3% conversion, using a ruthenium dye sensitizer (N3 dye, Figure 2.3) which contained one ruthenium center and was thus simpler than the ruthenium dye reported in 1991.

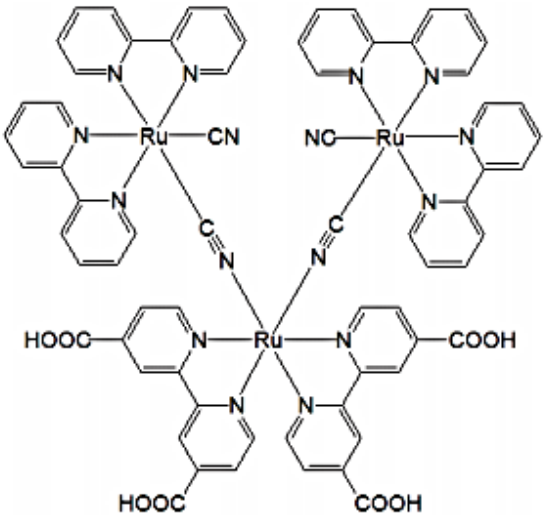

Figure 2.2 Molecular structure of ruthenium dye reported by O'Regan and Grätzel [4]

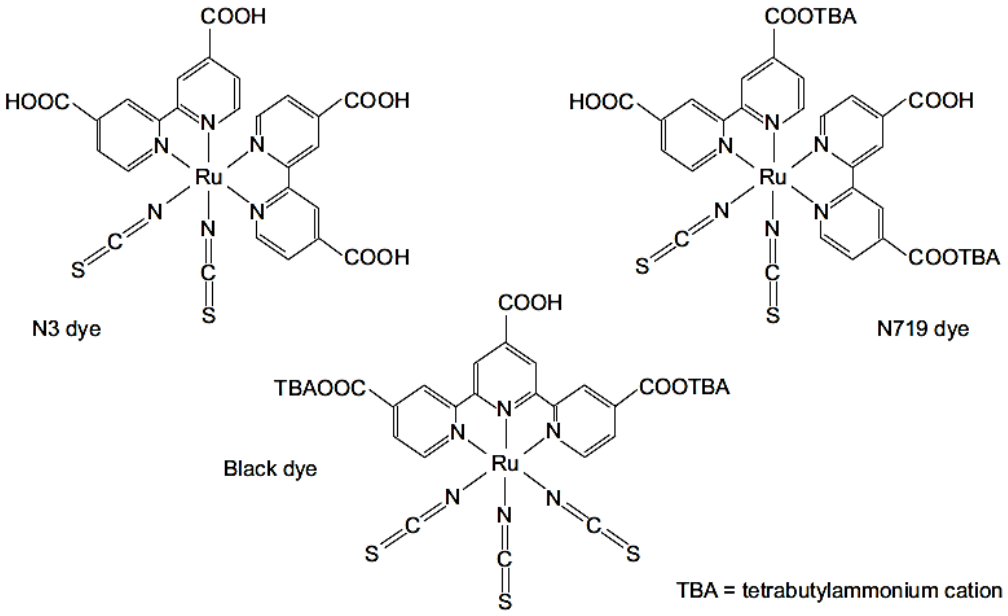

Figure 2.3 Structures of the ruthenium-based dyes N3, N719 and 'black dye' developed by the Grätzel group [22]

However, In 2001, Nazeeruzzin et al. [23] reported DSSCs with 10.4% efficiency using a ruthenium dye called 'black dye' in the Journal of the American Chemical Society (Figure 2.3). Although black dye looks green in solvent, on a porous nanocrystalline-TiO_2 electrode the DSSC looks black, because its wide absorption band covers the entire visible range of wavelengths. Subsequently, using black dye, In 2006, Nazeeruzzin et al. [24] reported a new dye, N179, which was similar to N3, but which achieved an 11.2% conversion efficiency in DSSCs. N3 has four H^+ counter ions, whereas N719 has three TBA^+ and one H^+ counter ions (Figure 2.3). The change in the counter ions alters the speed of adsorption onto the porous TiO_2 electrode; N3 is fast (3 hours) whereas N719 is slow (24 hours, thus N719 gives a higher conversion efficiency than N3.

2.1.4 Electrolyte

The best working redox-couple known so far is the iodide/triiodide system. The most efficient DSSCs have been constructed with the I^-/I_3^- redox couple dissolved in volatile organic solvents. The unique performance of I^-/I_3^- based liquid electrolytes is mainly attributed to the favorable penetration into the nanoporous semiconductor

film, very fast dye regeneration, and relatively slow recombination losses through reaction with injected photoelectrons. However, there are several negative features limiting industrial application of the I^-/I_3^- redox-couple: (1) iodine is extremely corrosive toward metals such as copper or silver, which are used as current collectors in some DSSCs; (2) iodine has a relatively high vapor pressure, which makes proper encapsulation of the cells challenging; (3) the I_3^- ion absorbs a significant part of visible light, stealing photons from the sensitizing dye; (4) the redox potential of the I^-/I_3^- limits the photo voltage. During the last two decades, a number of articles and reviews dedicated to the properties and behavior of the iodide/triiodide redox-couple have been published; [6, 25] in this review we will mainly focus on alternative redox-couples. The redox species used to transfer electron between the photoanode and counter electrode. Usually I^-/I_3^- couple is used as the redox mediator in DSSCs. The I_3^- produced due to regeneration of dye is reduced at the counter electrode by the reaction:

$$I_3^- + 2e^- \longleftrightarrow 3I^- \qquad (2.4)$$

On the other hand, the liquid electrolyte, namely iodide/triiodide (I^-/I_3^- redox couple), works well mainly due to its kinetic as shown in Figure 2.4 [26].

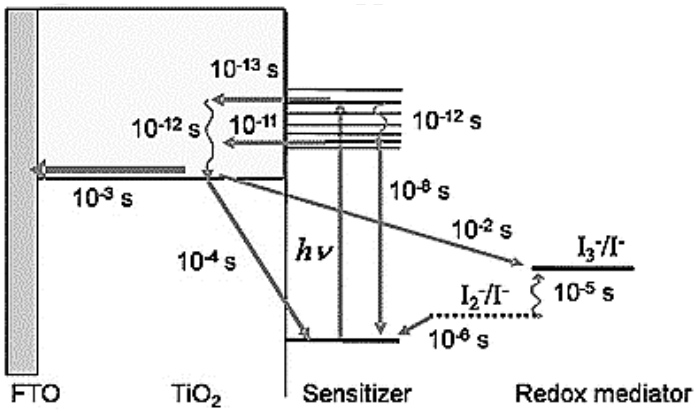

Figure 2.4 Kinetics of the cis-$Ru(dcbpy)_2(NCS)_2$-sensitized TiO_2 solar cell with I^-/I_3^- redox mediator. [26]

2.2 Operating principles

As the name implies, the mechanism of dye solar cells is based on the photo electrochemical processes. Figure 2.5 depicts an energy diagram of a dye solar cell. The following section describes all relevant electrochemical processes.

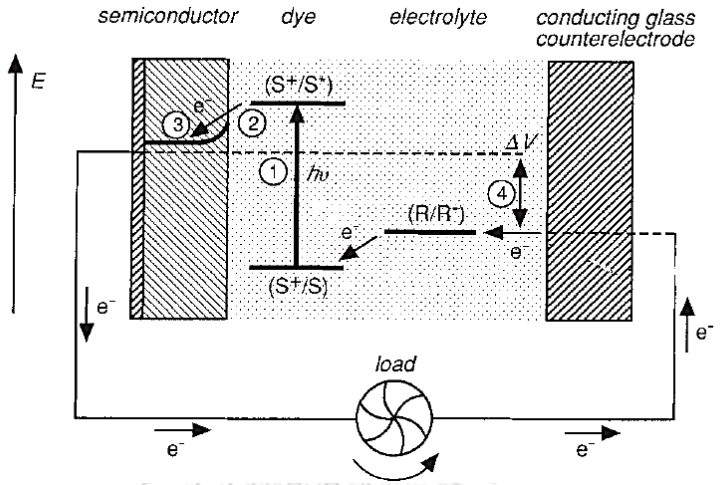

Figure 2.5 Operating principle and energy level diagram of dye-sensitized solar cell [4]

Step I The dye molecule is initially in its ground state (S). The semiconductor material of the anode is at this energy level (near the valence band) non-conductive.

When light shines on the cell, dye molecules get excited from their ground state to a higher energy state (S^*), see equation 2.5.

$$S \xrightarrow{h\nu} S^* \qquad (2.5)$$

The excited dye molecule has now a higher energy content and overcomes the band gap of the semiconductor.

Step II The excited dye molecule (S^*) is oxidized (see equation 2.6) and an electron is injected into the conduction band of the semiconductor. Electrons can now move freely as the semiconductor is conductive at this energy level.

$$S^* \xrightarrow{h\nu} S^+ + e^- \qquad (2.6)$$

Electrons are then transported to the current collector of the anode via diffusion processes. An electrical load can be powered if connected.

Step III The oxidized dye molecule (S^+) is again regenerated by electron donation from the iodide in the electrolyte (see equation 2.7).

$$S^+ + \frac{3}{2}I^- \xrightarrow{h\nu} S + \frac{1}{2}I_3^- \qquad (2.7)$$

Step IV In return, iodide is regenerated by reduction of triiodide on the cathode (see equation 2.8).

$$\frac{1}{2}I_3^- + e^- \xrightarrow{h\nu} \frac{3}{2}I^- \qquad (2.8)$$

2.3 Characteristic of photovoltaic cell

There are three significant parameters which are used to calculate the power conversion efficiency of DSSC are discussed in the following part such as the short-circuit current (I_{sc}), Open-circuit voltage (V_{oc}), and the fill factor (FF). All of parameter can be computed by using I-V curve. [27, 28]

As its name, I-V characteristic curve show the relationship between the current flowing through an electronic device and the applied voltage across its terminals.

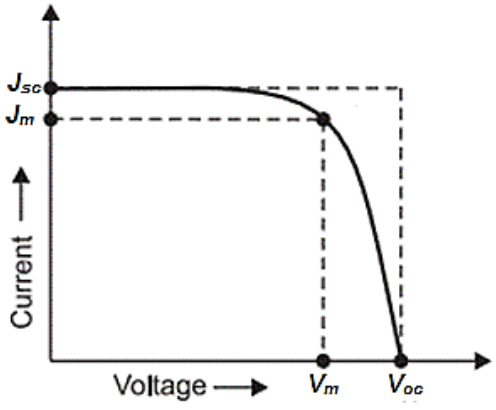

Figure 2.6 IV-curve for photovoltaic cell

2.3.1 Short-circuit current (J_{sc})

The short-circuit current is the current through the solar cell when the voltage across the solar cell is zero (i.e., when the solar cell is short circuited).

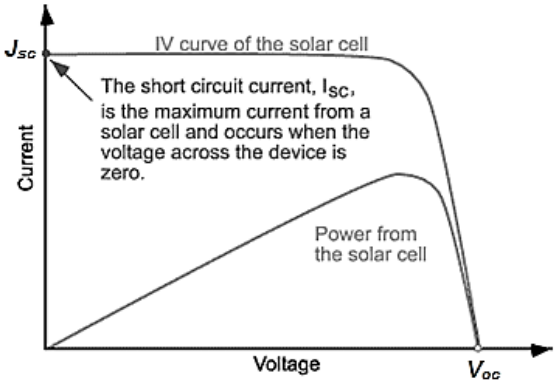

Figure 2.7 IV curve of a solar cell showing the short-circuit current

In order to compare with another cell, it is more common to use the short-circuit current density (J_{sc} in mA/cm^2) rather than short-circuit current. Short-circuit current (I_{sc} in mA) by dividing the area of the solar cell. The short-circuit current is due to the generation and collection of light-generation carriers. Normally, the Short-circuit current (I_{sc}) and the light-generated current (I_L) are alike. Therefore, the short-circuit current value of J_{sc} can be determined by integrating the total incident photon to current efficiency (IPCE) and incident photoflux over the spectral distribution.

When comparing solar cells of the same material type, the most critical material parameter is the diffusion length and surface passivation. In a cell with perfectly passivated surface and uniform generation, the equation for the short-circuit current can be approximated as:

$$J_{sc} = qG\ (L_n + L_P) \tag{2.9}$$

Where G is the generation rate, and L_n and L_p are the electron and hole diffusion lengths respectively. Although this equation makes several assumptions which are not true for the conditions encountered in most solar cells, the above equation

nevertheless indicates that the short-circuit current depends strongly on the generation rate and the diffusion length.

2.3.2 Open-circuit voltage (V_{oc})

The open-circuit voltage is the maximum voltage available from a solar cell, and this occurs at zero current. The open-circuit voltage corresponds to the amount of forward bias on the solar cell due to the bias of the solar cell junction with the light-generated current.

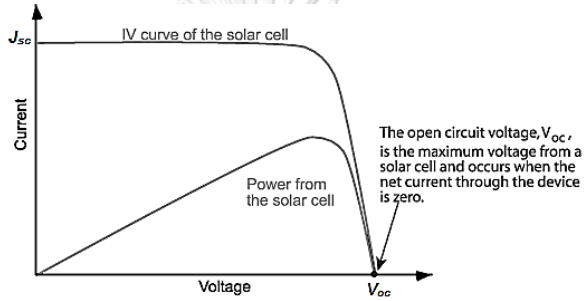

Figure 2.8 IV curve of a solar cell showing the open-circuit voltage.

An equation for V_{oc} is found by setting the net current equal to zero in the solar cell equation to give:

$$V_{oc} = \frac{kT}{q} \ln\left(\frac{I_{inj}}{I_{dark}} + 1\right) \qquad (2.10)$$

In the band gap theory, the difference between the quasi-Fermi level of the TiO_2 layer and the electrolyte redox potential determines the maximum voltage generated under illumination. The above equation show that V_{oc} relates to the dark current and the injection current. The injection current typically has a small variation whereas the dark current is a key effect to V_{oc} in fact, dark current is mainly due to the recombination at the TiO_2/dye and TiO_2/electrolyte interface where no photosensitizer got adsorbed. Suppressing of dark current enhances the open circuit voltage of the

solar cell. Hence, open-circuit voltage are used to describe the amount of recombination in the photovoltaic device.

2.3.3 Fill factor (FF)

The short-circuit current and the open-circuit voltage are the maximum current and voltage respectively from a solar cell. However, at both of these operating points, the power from the solar cell is zero. The "Fill factor", more commonly known by its abbreviation "FF", is a parameter which, in conjunction with V_{oc} and J_{sc}, determines the maximum power from a solar cell. The FF is defined as the ratio of the maximum power from the solar cell to the product of V_{oc} and J_{sc}. Graphically, the FF is a measure of the "squareness" of the solar cell and is also the area of the largest rectangle which will fit in the IV curve (refer to Figure 2.6).

$$FF = \frac{P_{MAX}}{P_T} = \frac{V_{MP} J_{MP}}{V_{OC} J_{SC}} \tag{2.11}$$

Where P_{MAX} is the maximum power output (W/cm^2), J_{MP} is the maximum current, and V_{MP} is the maximum voltage.

2.3.4 Photovoltaic efficiency

The efficiency is the most commonly used parameter to compare the performance of one solar cell to another. Efficiency is defined as the ratio of energy output from the solar cell to input energy from the sun. In addition to reflecting the performance of the solar cell itself, the efficiency depends on the spectrum and intensity of the incident sunlight and the temperature of the solar cell. Therefore, conditions under which efficiency is measured must be carefully controlled in order to compare the performance of one device to another. Terrestrial solar cells are measured under AM 1.5 conditions and at room temperature.

The efficiency of a solar cell is determined as the fraction of incident power which is converted to electricity and is defined as:

$$\eta = \frac{V_{OC} J_{SC} FF}{P_{in}} \times 100\,\%$$

(2.12)

When V_{oc} is the open circuit voltage (V), J_{sc} is short current density (mA/cm^2), FF is the fill factor and P_{in} is the incident light power (W/cm^2)

CHAPTER 3
LITERATURE REVIEWS

This chapter presented the literature review associated with dye-sensitized solar cell

3.1 Modification of TiO_2 electrode with mixed metal oxide

3.1.1 Modification of TiO_2 electrode with copper oxide

Zhou et al. [29] successfully prepared Cu-doped TiO_2 nanoparticle photoanode to improve the performance of dye-sensitized solar cells (DSSCs). Cu-doped TiO_2 powders were synthesized by a hydrothermal method and were printed onto fluorine-doped tin oxide. At the optimum Cu concentration of 1.0 at.%, the short circuit current density increased from 12.54 to 14.98 mA/cm^2, full sun solar power conversion efficiencies increased from 5.58% up to 6.71% as comparedto the blank DSSC. This showed that the presence of copper in DSSCs leads to improvements of up to 20% in the conversion efficiency of DSSCs.

Obina et al. [30] reported the cell of Cu/TiO_2 nanoparticle was deposited on the FTO glass used the spin coating method. Layers of Cu/TiO_2 nanocomposite were prepared in variations at 1, 2 and 3 layers. UV-VIS result was showed that there increased absorption wavelength of Cu/TiO_2 nanocomposite and were able to decrease the energy gap. The Cu/TiO_2 nanocomposite was showed that the highest efficiency in the 3 layers of Cu/TiO_2 nanocomposite of 0.011%.

3.1.2 Modification of TiO_2 electrode with nickel oxide

Sahu and Tarr [31] reported a facile way to fabricate three-dimensional (3D) Ni–TiO_2 core–shell nanowire arrays through anodic aluminum oxide templateassisted sol–gel TiO_2 nanotube shell growth followed by Ni core using room temperature constant current electrodeposition. The 3D Ni–TiO_2 nanowire-based dye-sensitized solar cell

(DSSC) endows a 67% increase in conversion efficiency as compared with the TiO_2 nanotube DSSC and maximum conversion efficiency of 5.07% was obtained by surface treating the photoanode with $TiCl_4$, which provides enhanced light scattering and surface passivation. Indeed, this work paves the way to build reliable 3D Ni–TiO_2 nanostructured photoanodes for highly efficient DSSCs.

Sakthivel et al. [32] prepared pure TiO_2 and Ni doped TiO_2 as photoanode material, dye sensitized solar cells (DSSCs) are fabricated with ruthenium complex as dyesensitizer [Cis-bis(isothiocyanato) bis(2, 2′-bipyridyl-4, 4′-dicarboxylato)ruthenium(II) also called as N3 dye] and LiI as redox electrolyte. In this concern, pure TiO_2 and Ni–TiO_2 are prepared through sol–gel technique. The electron transport properties of the prepared TiO_2 and Ni doped TiO_2 shows higher conductivity in 3% Ni doped TiO_2 confirmed from impedance studies. The interfacial charge transport resistances and chemical capacitances of the fabricated DSSCs are evaluated from the EIS investigations and the photovoltaic performance of Ni doped TiO_2 based DSSC shows enhanced efficiency up to 4%.

3.1.3 Modification of TiO_2 electrode with indium oxide

Chen et al. [33] reported the transparent In_2O_3–TiO_2 composite thin films in nanoscales were prepared via sol–gel method on the float glass substrates. It was found that the addition of In_2O_3 to TiO_2 thin films could suppress the grain growth of TiO_2 crystals and increase the surface smooth degree, the conductivity, carriers, concentration, and mobility of the as-prepared TiO_2 films. The band gap energy of the as-prepared In_2O_3–TiO_2 composite thin films increases from 3.36 eV to 3.44 eV with the increment of In-ingredient in the precursor sols, which provides the potential application of the as-prepared composite thin film using as the anode of the dye-sensitized solar cells to improve the open-circuit voltage.

The Hall-effect testing results are shown in Table 3.1. The sheet Hall coefficients of In_2O_3–TiO_2 composite films are negative, which reveals the prior conducting type is electron conduction. It is known that undoped TiO_2 is almost insulating and its

resistance exceeds the max limitation of Hall testing device. The addition of In_2O_3 decreases the resistance (sheet R) and increases the conductivity, carriers' concentration (sheet N) and mobility of TiO_2 films comparing with undoped TiO_2 films. These results shall enhance the properties of solar cell when the as-fabricated film is used as the anode of solar cell.

Table 3.1 The Hall testing results of samples with Ti/In = 1:0.03 and 1:0.06

Sample (Ti/In)	Sheet R (Ω/□)	Sheet Hall coefficient (m^2/C)	Sheet N (cm^{-2})	Mobility (cm^2/Vs)
1:0.06	120.0	−0.58	-1.07×10^{15}	48.4
1:0.12	159.0	−0.71	-8.84×10^{14}	44.4

3.2 The multi-layered structure of TiO_2 electrode of DSSCs

Hwang et al. [34] investigated the influences of dye-concentration for scattering layer in a dye-sensitized solar cell (DSSC), which is consisted with N719 dye on a bilayer anode with 250 nm-sized TiO_2 film onto 20 nm sized TiO_2 film, and compared to a monolayer anode 20 nm-sized TiO_2 film. The photovoltaic conversion efficiency of DSSC with the bilayer anode including a light-scattering layer (LSL-DSSC) was enhanced markedly compared to that of the DSSC with normal transparent layer anode (NTL-DSSC). This implies that the light-scattering layer increased the light amount absorbed by dyes. The photovoltaic conversion efficiency was improved more than 80% in low concentration of dye adsorbed on TiO_2, which is caused by the penetrating light up to the scattering layer.

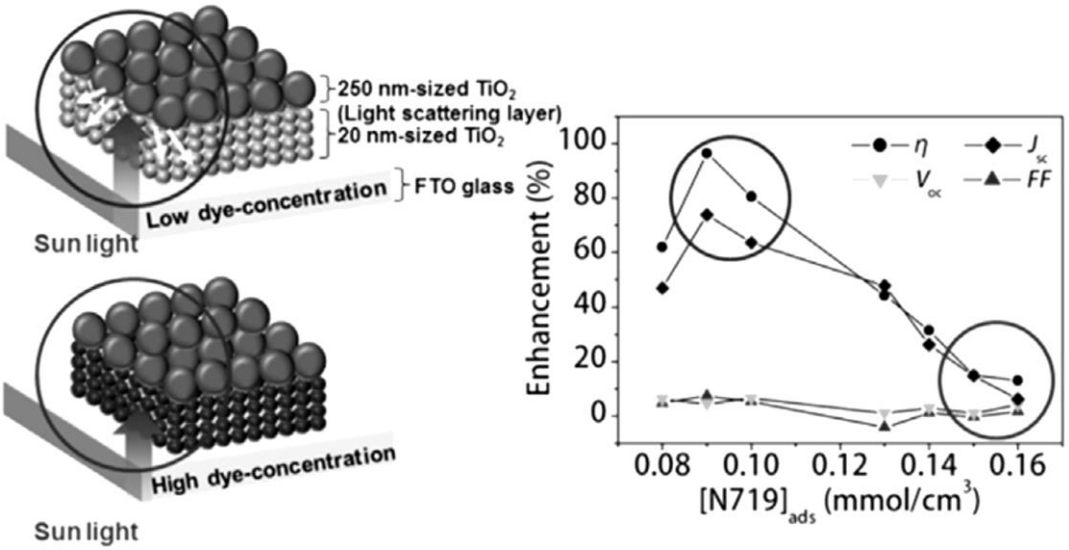

Figure 3.1 Schematics of the scattering layer in a dye-sensitized solar cell, which is consisted with N719 dye on a bilayer anode with 250 nm-sized TiO_2 film onto 20 nm sized TiO_2 film, and compared to a monolayer anode 20 nm-sized TiO_2 film. [34]

Choi et al. [35] fabricated multilayer structure using 15 and 250 nm particles. The TiO_2 powders were deposited with a subsonic nozzle at room temperature. Without sintering process enables to fabricate TiO_2 layer on the flexible polymer substrate. The multi-layer structure of semiconductor oxide can proved the bonding between electrode and semiconductor oxide layer and the interaction between semiconductor oxide and electrolyte. With these improvements, J_{SC} was increased and energy conversion efficiency of fabricated DSSC was increased 0.33 to 0.64%.

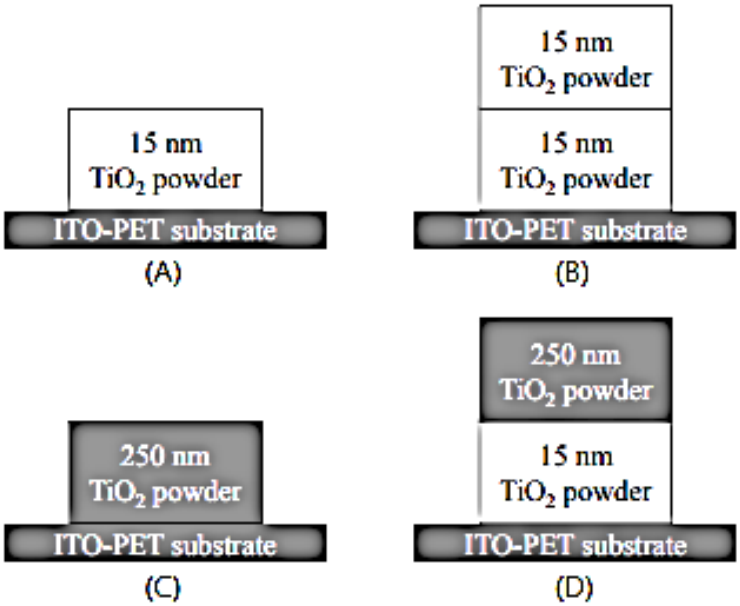

Figure 3.2 Schematic diagram of prepared TiO_2 layers. (A) is 15 nm TiO_2 monolayer, (B) is multi-layer by same particle size 15 nm, (C) is 250 nm TiO_2 monolayer, and (D) is multi-layer using 15 nm and 250 nm TiO_2 particles. [35]

Chou et al. [36] investigated the applicability of a hybrid TiO_2 electrode in a dye-sensitized solar cell (DSSC). Microcrystalline TiO_2 particles, synthesized by the simple sol–gel method. This study shows that the power conversion efficiency of the DSSC with a hybrid TiO_2 electrode (7.02%), which consisted of 50% TiO_2 particles (P-25) and 50% TiO_2 particles with an average size of 268.7 nm, substantially exceeds that of the conventional DSSC with a TiO_2 (P-25) electrode (5.16%) due to the effect of the light scattering in the DSSC.

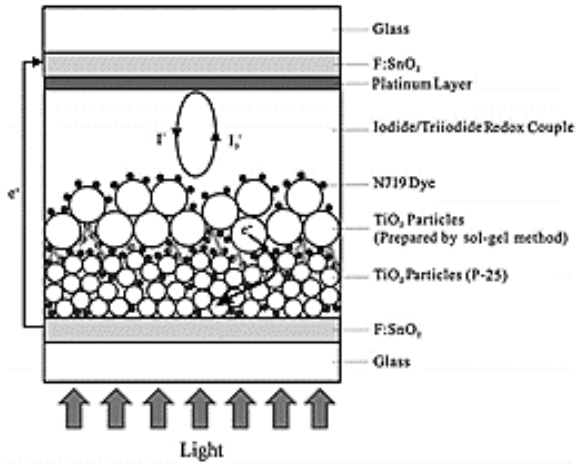

Figure 3.3 Dye-sensitized solar cell with a layer of TiO_2 particles (P-25) and a layer of TiO_2 particles prepared by the sol–gel method [36]

CHAPTER 4
EXPERIMANTAL

This chapter referred to all materials and methods in this research. The experiments involved in five sections: (I) materials (II) preparation of TiO_2 film and modified TiO_2 film electrodes (III) preparation of various DSSC components (VI) fabrication of dye-sensitized solar cells. (V) physical and electrochemical characterization.

4.1 Chemicals used in the study

Titanium tetraisopropoxide ($Ti[OCH(CH_3)_2]_4$, TTIP), nitric acid 70% (HNO_3), indium(III) nitrate hydrate ($In(NO_3)_3{\cdot}xH_2O$), lithium iodide (LiI), Iodine (I_2), 4-tert-butylpyridine (4-TBP), and sodium hydroxide (NaOH) were purchased from Sigma-Aldrich Inc. Copper (II) nitrate trihydrate ($Cu(NO_3)_2{\cdot}3H_2O$) was purchased from Honeywell Fluka. Acetonitrile (C_2H_3N) and acetone (C_3H_6O) were purchased from Labscan Ltd. Nickel(II) nitrate hexahydrate ($Ni(NO_3)_2{\cdot}6H_2O$) was purchased from Ajax Finechem Pty Ltd. Fluorine-doped tin oxide (FTO) conducting glass with a thickness of 2 mm and a resistance of 15 Ω/cm^2 fluorine doped tin oxide coating on one side, surlyn film (25 μm thick sealing film), cis-bis(isothiocyanato) bis(2,2′-bipyridyl-4,4′-dicarboxylato) ruthenium(II) dye (also known as N3), and di-tetrabutylammonium cis-bis(isothiocyanato) bis(2,2′-bipyridyl-4,4′-dicarboxylato) ruthenium(II) dye (also known as N719) were purchased from Solaronix SA (Switzerland).

4.2 Preparation of TiO_2 and modified TiO_2 sols

4.2.1 Preparation of TiO_2 sol

TiO_2 was synthesized via a sol-gel method by mixing the starting titanium isopropoxide (TTIP) in deionized water that contained 70% nitric acid as a catalyst. The volume ratio between TTIP, deionized water, and nitric acid was 1:12:0.087. After adding TTIP a white precipitate was instantaneously formed. The mixture was

vigorously stirred for three days at room temperature until clear sol was obtained. Then the clear sol was dialyzed in cellulose membrane with a molecular weight cutoff of 3500. The distilled water used for dialysis was changed daily until a pH of sol reached to 3.5. Finally, TiO_2 sol was kept into refrigerator until further used.

4.2.2 Preparation of modified TiO_2 sols

In this research, the precursor was dissolved in deionized water. After its pH was adjusted to 3 using 5 M of nitric acid, the solution was then added to TiO_2 sol according to desire amount of metal oxide at 0, 0.1, 0.5, 1.0, and 3.0%wt. while being stirred for 30 minutes. Homogeneous sol was obtained at room temperature until further use in the spray coating process.

Table 4.1 Preparation of metal oxide doped TiO_2 sol in various percentage

Resulting sol	Precursor	%wt.	volume of precursor solution (ml)	volume of TiO_2 sol (ml)
CuO/TiO_2	0.5 g of $Cu(NO_3)_2 \cdot 3H_2O$ in 50 ml of DI water	0.1	0.25	49
		0.5	1.21	48
		1.0	2.38	47
		3.0	7.13	46
NiO/TiO_2	0.5 g of $Ni(NO_3)_2 \cdot 6H_2O$ in 50 ml of DI water	0.1	0.32	49
		0.5	1.55	48
		1.0	3.05	47
		3.0	9.15	46
In_2O_3/TiO_2	0.5 g of $In(NO_3)_3 \cdot xH_2O$ In 50 ml of DI water	0.1	0.18	49
		0.5	0.86	48
		1.0	1.70	47
		3.0	5.08	46

Note: TiO_2 sol 100 ml = TiO_2 1.65 g

4.3 Preparation of DSSC components

4.3.1 Preparation of ruthenium dye solutions

To prepare the solution of N3 or N719, ruthenium-based N3 or N719 dye was weighed and was dissolved in ethanol to obtained 0.3 mM. The mixture was sonicated in an ultrasonic bath for 30 minutes until a homogeneous solution was obtained.

4.3.2 Preparation of electrolyte solution

The electrolyte solution was a mixture of 0.5 M lithium iodide, 0.05 M iodine, and 0.5 M 4-tert-butylpyridine in acetonitrile. The electrolyte solution prepared by mixed 2 g of lithium iodide (LiI) , 0.38 g of iodine (I_2), and 2.20 mL of 4-tert-butylpyridine (4-TBP) in 30 mL of acetonitrile (Molar ratio LiI:I_2:4-TBP = 0.1:0.01:0.1). The mixed solution was stirred for 30 minutes until homogeneity was obtained.

4.3.3 Preparation of TiO_2 photoanode or modified/TiO_2 electrode

FTO glass was cut into pieces with a dimension of 2.0 × 2.5 cm^2. The glass pieces cleaned three times with detergent solution, acetone, and ethanol, respectively, using ultrasonic bath for 15 minutes in each step. Fingerprints were wiped off using a tissue wetted with ethanol and dried with blow dryer. Then the glass was covered with aluminum foil that was cut in a circular shape with a diameter of 0.5 cm. The schematic diagram of the electrode is displayed in Figure 4.1.

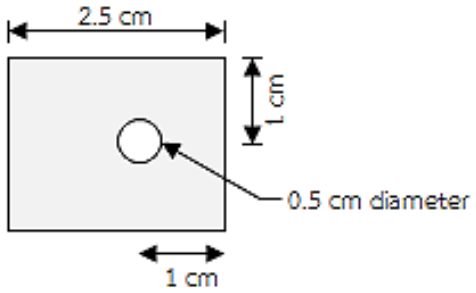

Figure 4.1 The counter electrode before spray coating

After that, TiO_2 or modified/TiO_2 sol was deposited on the FTO glass using an ultrasonic spray coater. The liquid feed rate to ultrasonic nozzle for TiO_2 or metal

oxide/TiO_2 sol was set at 1 mL/min. The power for frequency generator of ultrasonic nozzle was set at 3.5-3.6 W.

In this research, the number of layers of metal oxide/TiO_2 was 500 coats, which produced a film with a thickness of approximately 10 μm. An electrode was sintered at 400°C for two hours and left to be cooled at room temperature.

Prior to dye immersion, an electrode was gradually heated to 110°C and was held for 10 minutes to remove water. Then the electrode was slowly slid into a solution of ruthenium-based N3 dye for 20-24 hours in the dark. Finally, the electrode was washed with ethanol to remove excess dye and was dried with a blow dryer

4.3.4 Preparation of platinum film counter electrode

The counter electrode was prepared on FTO glasses, which was cut into pieces with a dimension of 2.0 × 2.5 cm^2. Then two small holes with a diameter of 1 mm was carefully drilled through the FTO glass for subsequent filling of electrolyte solution. Next, the FTO glass was cleaned in the same manner as described in Section 2.4. The platinum film was deposited on the FTO glass using ion sputtering machine (JEOL: JFC-1100E) at 10 mA of ion current for six minutes. Sputtering area was 2.0 × 2.0 cm^2 in size. The schematic diagram is displayed in Figure 4.2.

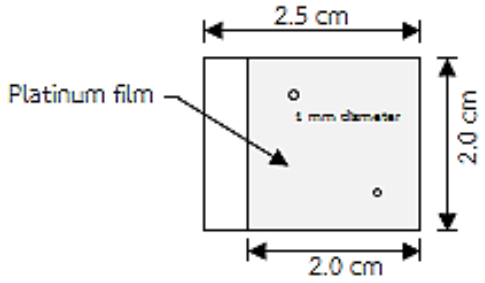

Figure 4.2 The schematic diagram of platinum film counter electrode

4.4 Fabrication of dye-sensitized solar cells

The DSSC was configured in a typical sandwiched cell by placing a TiO_2 or metal oxide/TiO_2 electrode on the top of platinum film counter electrode with a 25 μm thick

surlyn film inserted in the middle. The sealing material was cut into a square with a dimension of 2.0 × 2.0 cm^2 and square hole was made in the middle of the film, leaving a square frame.

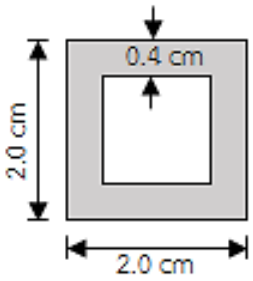

Figure 4.3 The sealing material as a sealant between two electrodes

The two electrodes with sealing sheet were clipped together with 2 clips on the opposite end of the glass. The surlyn film was softened by a heat gun and the sealing effect was obtained. To add the electrolyte solution, the solution was added dropwise until both holes were completely filled. The arrangement of the DSSCs component is shown in Figure 4.4. After that both holes were sealed off by a clear adhesive tape to prevent the electrolyte solution from leaking. The resulting cell was ready for a measurement.

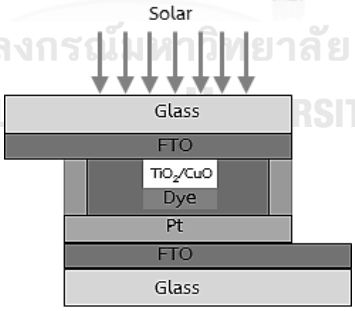

Figure 4.4 Fabrication of DSSC assembly for testing

4.5 Physical and electrochemical characterization

4.5.1 X-ray diffractometry (XRD)

The crystalline phase and crystallite size of TiO_2 and metal oxide/TiO_2 was determined using a SIEMENS D5000 X-ray diffractometer with CuKα radiation (λ =

1.54439 Å) and Ni filter. The spectrum was scanned at a rate of 0.04 min^{-1} in the 2Θ range of 20-80°.

4.5.2 N_2 physisorption

N_2 physisorption was performed using a Micromeritics ASAP 2010 to determine the specific area from the BET isotherm. The cumulative volume of pores and average pore diameter were estimated from the total amount of N_2 desorption by using BJH method.

4.5.3 UV-Visible spectroscopy (UV-Vis)

- Determine the amount of dye adsorbed on photoanode electrode

The peak light absorption wavelengths of ruthenium-based N3 or N719 dyes were determined by UV-Visible spectrophotometer (Perkin Elmer Lambda 650 spectrophotometer) to be 314 nm for N3 dye and 312 nm for N719. To determine the amount of dye adsorbed on the metal oxide/TiO_2 film, the dye was dissolved in a solution of 0.1 M of NaOH in DI water and ethanol (1:1 volume fraction). The concentration of dye in the solution was later determined using UV-visible spectroscopy.

- Determine the band gap energy of catalysts and reflection of electrodes

The light absorption of the catalysts was evaluated by UV-Visible spectroscopy. The diffuse reflectance spectrum of the catalysts was obtained in the wavelength range of 200 to 800 nm with a step size of 1 nm. The band gap energy of the catalyst was estimated by equation (4.1)

$$E_g = \frac{1240}{\lambda} \qquad (4.1)$$

When E_g is the band gap energy (eV) of the catalyst and λ is the wavelength at which the absorption begins (nm).

The UV-Vis spectrum can be used to calculate the band gaps of semiconductor material (allowed direct, allowed indirect, forbidden direct, and forbidden indirect transitions), by plotting the graph between $(\alpha h\nu)^{(1/n)}$ versus photon energy ($h\nu$) where a: is the optical absorption coefficient, which can be calculated from absorbance (A), and thickness of the sample (t) using: (α =2.303A/t); and ($h\nu$) can be calculated from wavelength using: ($h\nu$ = 1240/wavelength); The power factor (n) takes the values of (0.5, 2, 1.5, and 3) for allowed direct, allowed indirect, forbidden direct and forbidden indirect transition

4.5.4 Inductively couple plasma-atomic emission spectroscopy (ICP-AES)

The amount of metal deposited on the surface of TiO_2 was measured with Optima 2100 DV spectrometer. A powder of catalyst was digested into solution phase. First, we dissolved 0.05 g of catalyst with 7 ml of 97% H_2SO_4. Next, 2.7 g of $(NH_4)_2SO_4$ was added into solution while being stirred until homogenous solution was obtained. Then the resulting solution was made up to 50 ml with deionized water. The solution is ready to measure and compare with a calibration curve to obtain an amount of metal loading.

4.5.5 Current-voltage tester (I-V tester)

The electrochemical properties of DSSC were determined by an IV-tester under air mass (AM) 1.5 condition (Keithley's 2420 source meter). The current-voltage characterization of DSSCs was conducted under simulated sun illumination. The short current density (J_{sc}), open circuit voltage (V_{oc}), and fill factor (FF) were determined and this information was then converted to the efficiency of a DSSC (η). An area of our solar cell was 0.196 cm^2. The efficiency of DSSC (η) was determined by equation (4.2)

$$\eta = \frac{V_{OC} J_{SC} FF}{P_{in}} \times 100\,\% \qquad (4.2)$$

When V_{oc} is the open circuit voltage (V), J_{sc} is short current density (mA/cm^2), FF is the fill factor and P_{in} is the incident light power (W/cm^2)

CHAPTER 5
RESULTS AND DISCUSSION

5.1 Modification of TiO_2 electrode layer by using mixed metal oxide

5.1.1 Modification of TiO_2 electrode layer by adding CuO

CuO/TiO_2 sols were prepared by mixing different amounts of CuO and TiO_2 sols to obtain the CuO amounts of 0.1, 0.5, 1.0 and 3.0%wt. The CuO/TiO_2 sol was sprayed on the FTO glass substrates 500 times and was calcined at 400°C for two hours.

The XRD peaks detected at 2θ of 25.3°, 37.2°, 48.2°, and 62.8° were assigned to anatase TiO_2, whereas the peak at 27.4°, 41.3°, and 54.4° corresponded to rutile phase and the peak at 30.9° was associated to brookite. A mixture of anatase and rutile TiO_2 usually produces the DSSC that exhibits higher photovoltaic efficiency than pure anatase [37]. XRD patterns of CuO/TiO_2 were shown in Figure 5.1. No XRD peak associated with CuO was detected because of small amount of CuO adding in TiO_2 sol.

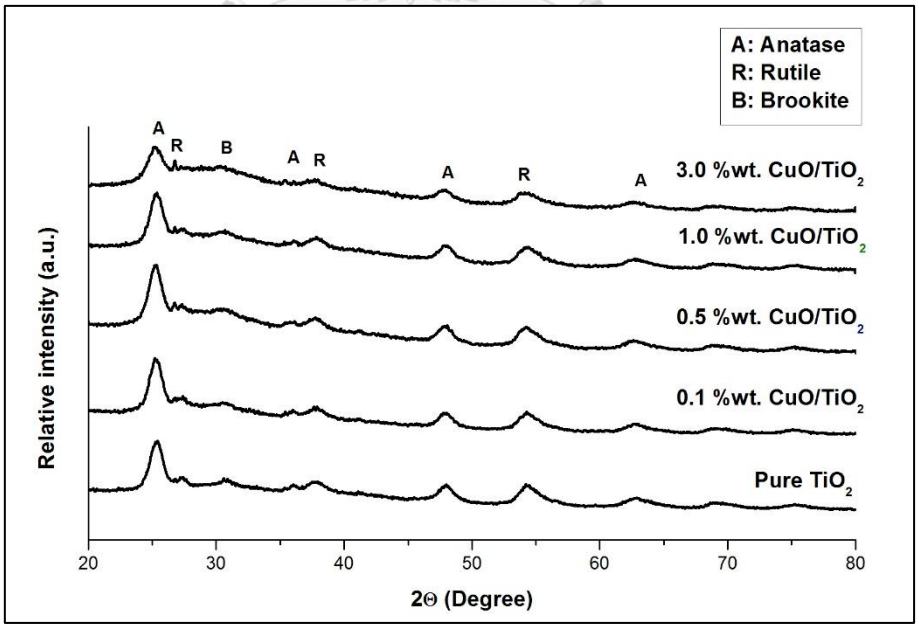

Figure 5.1 XRD patterns of CuO/TiO_2 powders at various percentages of CuO

The major phase in all samples was anatase with some rutile and very small amount of brookite. Table 5.1 lists the crystallite size of TiO_2 phase in CuO/TiO_2. Debye-

Scherer equation can be used to calculate the crystallite size (showed in Appendix A). The crystallite size of anatase phase in TiO_2 became smaller when the amount of CuO/TiO_2 was increased. To explain this results, the growth mechanism of pure TiO_2 nanoparticles was involved in the agglomeration of domain structure at grain boundaries whereas in the case of doped TiO_2 particles, this agglomeration of domain structure is restricted due to the insertion of atomic metal [37].

Weight fraction of TiO_2 was shown on Table 5.1. All sample composed of primarily anatase phase and small amount of rutile and brookite. The calculation of weight fraction phase of TiO_2 was shown in Appendix B. These results show that the transformation of anatase to rutile depends significantly on the CuO contents, and it seems that the dopant segregation occurs for CuO content up to 3.0%wt., which is responsible for the acceleration of the anatase-rutile transformation [38].

Inductively coupled plasma atomic emission spectroscopy (ICP-AES) was used to confirm the amount of CuO in TiO_2. The results was showed in Table 5.1 and calculated amount of metal oxide from ICP was showed in Appendix E. The results indicated that the content of CuO/TiO_2 was less than intended value because of error from digestion for sample powder, and error from preparation of modified/TiO_2 sols.

Table 5.1 Crystallite size and weight fraction of anatase, rutile and brookite of CuO/TiO_2 powder calcined at 400°C for 2 hours

Sample	Crystallite size (nm)	Amount of CuO from ICP (%wt.)	W_A	W_R	W_B
Pure TiO_2	8.3	-	0.73	0.23	0.03
0.1%wt. CuO/TiO_2	8.0	0.07	0.66	0.29	0.05
0.5%wt. CuO/TiO_2	7.5	0.43	0.56	0.43	0.01
1.0%wt. CuO/TiO_2	7.4	0.69	0.70	0.26	0.04
3.0%wt. CuO/TiO_2	6.7	2.23	0.68	0.31	0.01

The surface specific area and BJH pore properties were determined by the BET method in the CuO/TiO_2 nanoparticles calcined at 400°C listed in Table 5.2. Specific surface area, pore volume, and pore diameter of 0.1-1.0%wt. CuO/TiO_2 differed only slightly when compared to pure TiO_2, related to crystallite size. However, the 3.0%wt. CuO/TiO_2 presented lower surface specific area than other samples due to blocking or their own surface area of CuO.

Table 5.2 Specific surface area, pore volume, and average pore diameter of TiO_2 and CuO/TiO_2 that were calcined at 400°C for 2 hours

Sample	BET Surface area (m^2/g)	BJH Pore volume (cm^3/g)	BJH Pore diameter (nm)
Pure TiO_2	112.8	0.196	4.90
0.1%wt. CuO/TiO_2	113.3	0.178	4.05
0.5%wt. CuO/TiO_2	103.3	0.158	4.44
1.0%wt. CuO/TiO_2	109.4	0.186	4.71
3.0%wt. CuO/TiO_2	94.6	0.162	4.70

The band gap energy of pure anatase TiO_2 was 3.20 eV [39]. The band gap energies of various CuO/TiO_2 were determined from Figure 5.2 and were reported in Table 5.3. An increase in CuO/TiO_2 content reduced its band gap energy, resulting in ability to absorb light in the visible region. With a newly combined state because of the incorporation of CuO into the lattice, an absorption peak in the visible-light range occurred, and this absorption increased with increasing CuO content [40]. In case of DSSC, the band gap under 3.10 eV or absorption wavelength over 400 nm might not be suitable because it may prevent some photons from reaching the dye layer.

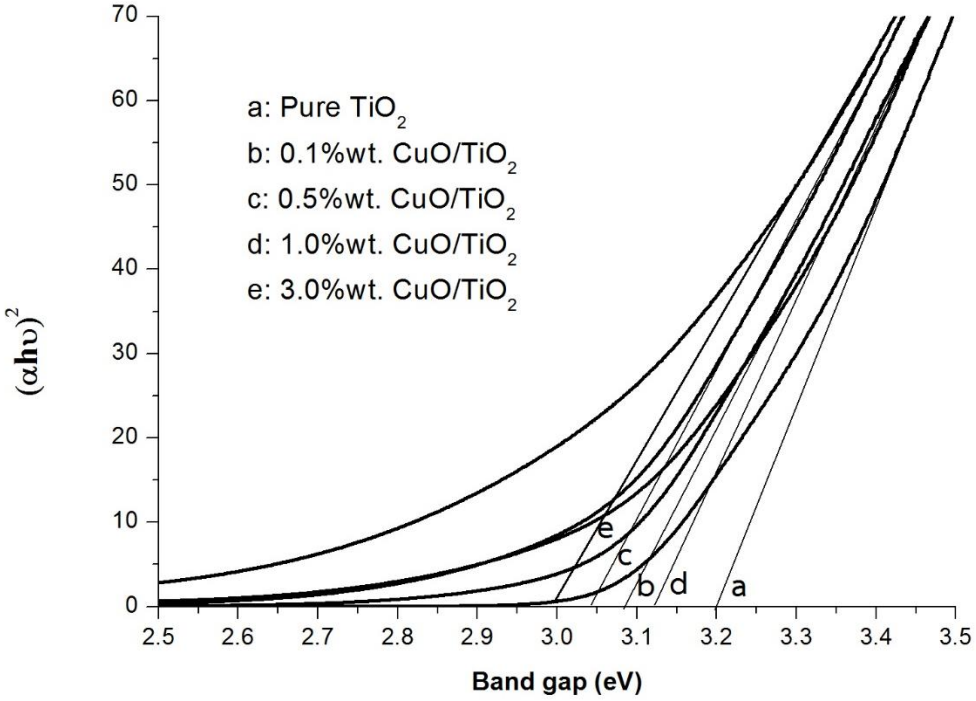

Figure 5.2 UV-visible adsorption characteristic of CuO/TiO_2

Table 5.3 Band gap energy of TiO_2 and CuO/TiO_2 that were calcined at 400°C for 2 hours

Sample	Wavelength (nm)	Band gap energy (eV)
Pure TiO_2	388	3.20
0.1%wt. CuO/TiO_2	403	3.08
0.5%wt. CuO/TiO_2	397	3.04
1.0%wt. CuO/TiO_2	408	3.12
3.0%wt. CuO/TiO_2	413	3.00

The amount of dye adsorbed on the CuO/TiO_2 film, the N3 or N719 dye was dissolved in a solution of 0.1 M of NaOH in deionized water and ethanol (1:1 volume fraction). The ruthenium-based dye solution was analyzed by UV-Visible spectrophotometer (314 nm for N3 dye and 312 nm for N719 dye). Three replicates dissolved dye adsorbed on photoanode and determine the corresponding of standard

deviation. The calculations of amount of dye adsorbed can be viewed in Appendix C. The amount of N719 or N3 dyes adsorbed on CuO/TiO_2 electrode was lower, compared to pure TiO_2 possibly because of smaller specific surface area, compare to pure TiO_2 possibly because of smaller specific surface area, but 0.1%wt. CuO/TiO_2 electrode was differed only slightly when compared to pure TiO_2. (see Table 5.4-5.5) therefore, it can be concluded that the amounts of adsorbed N3 dye corresponded to surface area of semiconductor.

Table 5.4 The concentration of N3 dye contained in the CuO/TiO_2 electrode at various content of CuO

Sample	Concentration of N3 dye ($\times 10^7$ mol/cm^2)
Pure TiO_2	1.39±0.003
0.1%wt. CuO/TiO_2	1.41±0.003
0.5%wt. CuO/TiO_2	1.04±0.008
1.0%wt. CuO/TiO_2	1.27±0.002
3.0%wt. CuO/TiO_2	1.20±0.003

Table 5.5 The concentration of N719 dye contained in the CuO/TiO_2 electrode at various content of CuO

Sample	Concentration of N719 dye ($\times 10^7$ mol/cm^2)
Pure TiO_2	1.52±0.007
0.1%wt. CuO/TiO_2	1.31±0.001
0.5%wt. CuO/TiO_2	0.74±0.044
1.0%wt. CuO/TiO_2	0.98±0.022
3.0%wt. CuO/TiO_2	1.07±0.006

Increasingly research into DSSC is addressing the use of more sophisticated device architectures in order to reduce interfacial recombination losses. Examples

include the use of composite metal oxides as the semiconductor with different band-gaps, the incorporation of spacer units between the oxidized dye and the TiO_2 surface, and surface passivation by electrodeposition of insulating polymers. One particularly attractive approach involves the coating of the nanocrystalline metal oxide film with a thin overcoat of another metal oxide with a higher conduction band edge, with the aim of increasing the physical separation of injected electrons for the oxidized dye redox couple, thereby retarding the recombination reactions [41]. The electron transfer from TiO_2 nanoparticles into electrolyte species is a complex phenomenon because it involves a combination of processes. First, there is a variety of electronic states from which electrons can be injected, both conduction band states and bandgap surface states that exhibit a wide distribution in energy. The transport of electrons in CuO/TiO_2 not good because of the conduction band of CuO was lower than the conduction band of TiO_2. The recombination of electrons can occur more easily. (see Figure 5.3)

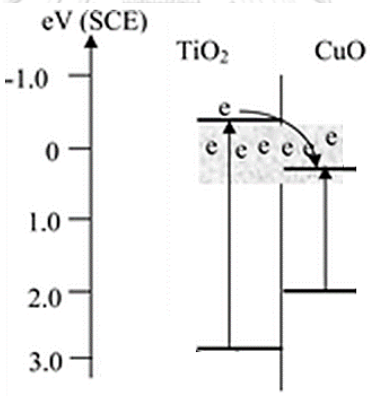

Figure 5.3 Schematic diagram showing the energy band positions of TiO_2/CuO and the electron transfer direction. [42]

The I-V characteristics and efficiencies of DSSC with TiO_2 and CuO/TiO_2 electrodes were listed in Table 5.6-5.7. Five replicates of DSSC with each CuO content were prepared and they were measured individually. The number displayed was the average value of five DSSCs value and the corresponding standard deviation.

In this research, N3 or N719 was employed as the dye for DSSC. CuO/TiO_2 content were prepared by sol-gel method and coated on top of Fluorine doped tin oxide (FTO) conductive glass and sintered at 400°C for two hours. After assembled with platinum counter electrode, the electrolyte solution was dropped in the space between the two FTO glasses. The DSCC was then measured its open circuit voltage (V_{oc}) and short-circuited current density (J_{sc}) under light source irradiation simulated AM 1.5 with the power density of 100 mW/cm^2. As seen in Table 5.4 the amount of adsorbed dye in pure TiO_2 and 0.1%wt. CuO/TiO_2 were higher than the rest, leading to higher conversion efficiencies for the DSSCs with pure TiO_2 and 0.1%wt. CuO/TiO_2. When the CuO content exceeded 0.1%wt., the amount of adsorbed dye decreased and consequently lowered the current density (J_{SC}) because lower conductive band [43]. The low efficiencies for DSSCs with CuO/TiO_2 electrode that contained CuO greater than 0.1%wt. may be attributed to this low current density. Due to the high amount of adsorbed dye, the highest cell efficiency of 4.03±0.58% was obtained with 0.1%wt. CuO/TiO_2 electrode coated by ruthenium-based N3 dye.

Table 5.6 Electrochemical properties of DSSCs with CuO/TiO_2 electrode coated with N3 dye and were sintered at 400°C for 2 hours

CuO/TiO_2 (%wt.)	**V_{oc} (Volt)**	**J_{sc} (mA/cm^2)**	**Fill Factor**	**Efficiency (%)**
0	0.68	6.89	0.72	3.40±0.62
0.1	0.67	8.19	0.73	4.03±0.58
0.5	0.67	4.95	0.63	2.08±0.41
1.0	0.68	3.50	0.65	1.55±0.38
3.0	0.68	2.30	0.68	1.06±0.06

Table 5.7 Electrochemical properties of DSSCs with CuO/TiO_2 electrode coated with N719 dye and were sintered at 400°C for 2 hours

CuO/TiO_2 (%wt.)	V_{oc} (Volt)	J_{sc} (mA/cm^2)	Fill Factor	Efficiency (%)
0	0.70	6.96	0.69	3.31±0.30
0.1	0.69	6.99	0.71	3.41±0.31
0.5	0.66	3.69	0.67	1.64±0.68
1.0	0.67	2.21	0.62	0.91±0.17
3.0	0.63	2.29	0.64	0.93±0.15

5.1.2 Modification of TiO_2 electrode layer by adding NiO

Nickel oxide-doped TiO_2 sols were prepared by sol–gel method in various percentage of NiO, 0.1, 0.5, 1.0 and 3.0%wt. The NiO/TiO_2 sol was sprayed on the FTO glass substrates 500 times and eventually sintered at 400°C for two hours. The TiO_2 decorated with NiO are extensively studied because they are low-cost, non-toxic and especially have wide applications. NiO is one of a p-type metal-oxide semiconductor. NiO thin films were used as a barrier layer at the photo-electrodes in order to control charge recombination dynamics. Also, NiO thin films were applied to the platinized counter electrodes in order to increase an active surface area [44-45]

Figure 5.4 shows the XRD pattern of TiO_2 and NiO/TiO_2 contents. The fraction phase of TiO_2 was calculated and shown in Appendix B. All samples were composed of anatase as major phase and small amount of rutile and brookite phase.

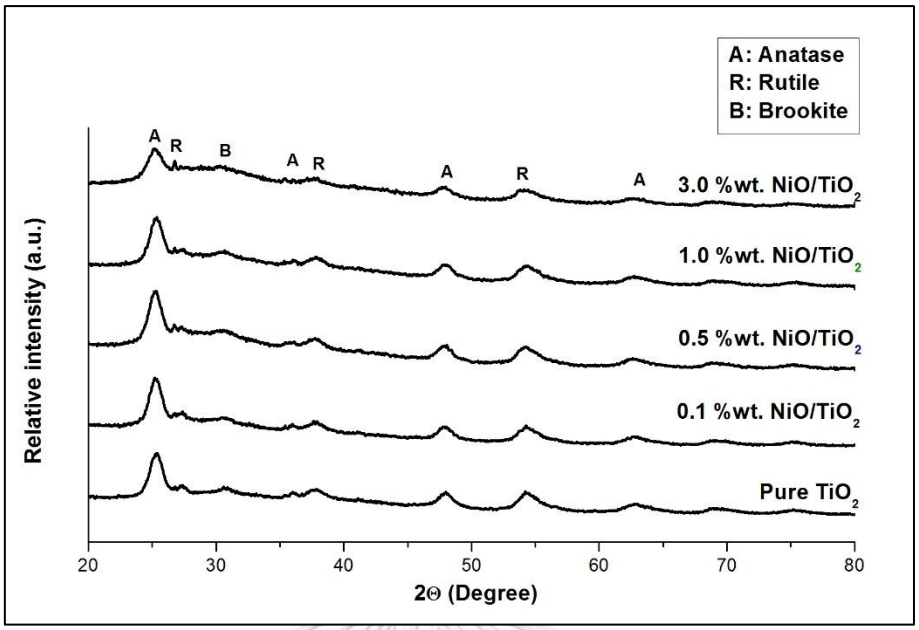

Figure 5.4 XRD patterns of NiO/TiO_2 powders at various percentages of NiO

The NiO/TiO_2 contents showed majorly anatase phase (60-70%) with crystallite size became smaller when the amount of NiO was increased. Thus, NiO inhibited TiO_2 crystalline growth, leading to small grain size. However, weight fraction of TiO_2 have been calculated thoroughly in number. The XRD results confirm that the addition of metal ions affects the anatase – rutile (A –R) transformation. The metal ions promote the A–R transformation. The influence of metal ion doping on the A –R transformation of the TiO_2 thin layers on metal oxide depends on the substitution of foreign ions for Ti^{4+} ions in TiO_2 thin layers. [46]

The amount of NiO was measured and calculated by ICP analysis. (see Table 5.8) The result of ICP shown the content of NiO/TiO_2 less than intended value because of the preparation of metal oxide mixed with TiO_2 sol or digestion of sample for ICP analysis.

Table 5.8 Crystallite size, surface area and weight fraction of anatase, rutile and brookite of NiO/TiO_2 powder calcined at 400°C for two hours

Sample	Crystallite size (nm)	Amount of NiO from ICP (%wt.)	W_A	W_R	W_B
Pure TiO_2	8.3	-	0.73	0.23	0.03
0.1%wt. NiO/TiO_2	7.6	0.06	0.61	0.34	0.05
0.5%wt. NiO/TiO_2	7.9	0.27	0.65	0.29	0.06
1.0%wt. NiO/TiO_2	7.3	0.63	0.64	0.31	0.05
3.0%wt. NiO/TiO_2	7.2	2.38	0.62	0.33	0.06

In Table 5.9 shown, the specific surface area and pore volume of 0.1 to 1.0%wt. NiO/TiO_2 were increased. The highest specific surface area is 0.5%wt. NiO/TiO_2 (123.7 m^2/g). However, the pore diameter of NiO/TiO_2 content differed only slightly.

Table 5.9 Specific surface area, pore volume, and average pore diameter of TiO_2 and NiO/TiO_2 that were calcined at 400°C for 2 hours

Sample	BET Surface area (m^2/g)	BJH Pore volume (cm^3/g)	BJH Pore diameter (nm)
Pure TiO_2	112.8	0.196	4.90
0.1%wt. NiO/TiO_2	118.1	0.246	4.92
0.5%wt. NiO/TiO_2	123.7	0.256	4.94
1.0%wt. NiO/TiO_2	117.4	0.227	4.90
3.0%wt. NiO/TiO_2	101.5	0.203	4.46

The band gap energy of NiO/TiO_2 were shown in Figure 5.5 and Table 5.10. The band gap was slightly widened to 3.02-3.15 eV for 0.1-3.0%wt. NiO/TiO_2. The results demonstrated that the absorption edge shifted towards visible region with the presence of NiO. In addition, the extension to visible region of the absorption edge reveals that good contact between NiO and TiO_2 in consequence of inter-dispersion of the two oxides [47].

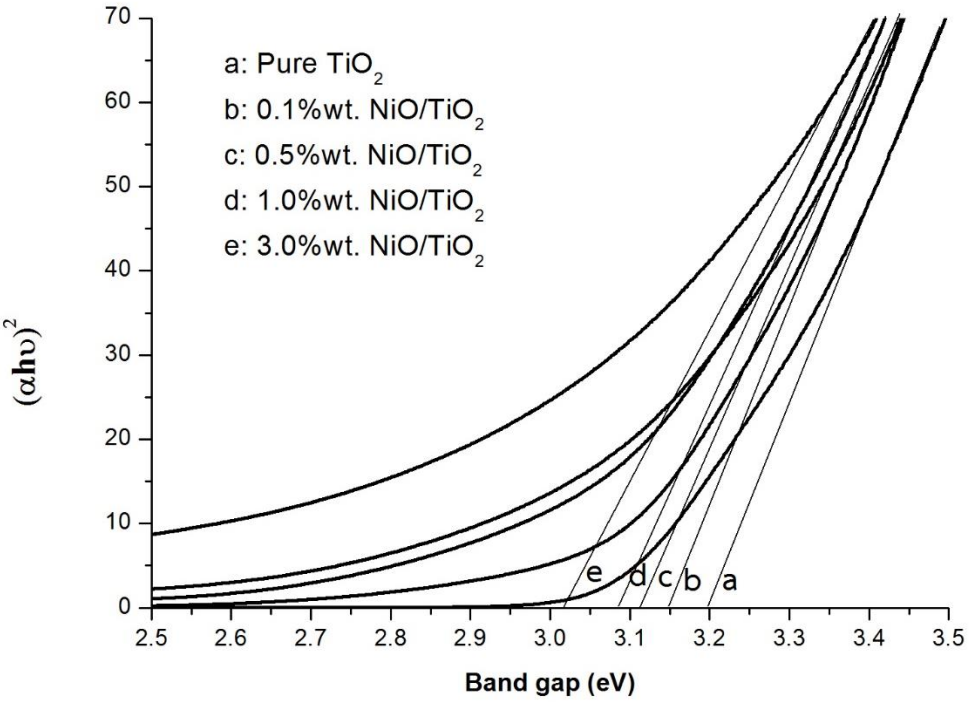

Figure 5.5 UV-visible adsorption characteristic of NiO/TiO_2

Table 5.10 Band gap energy of TiO_2 and NiO/TiO_2 that were calcined at 400°C for 2 hours

Sample	Wavelength (nm)	Band gap energy (eV)
Pure TiO_2	388	3.20
0.1%wt. NiO/TiO_2	394	3.15
0.5%wt. NiO/TiO_2	397	3.12
1.0%wt. NiO/TiO_2	401	3.09
3.0%wt. NiO/TiO_2	411	3.02

Table 5.11 showing the amount of N3 dye adsorbed on NiO/TiO_2 photoanode electrode. All sample can adsorb more dye and effect to support efficiency by enhanced the current density (J_{sc}) value. The BET specific surface area of NiO/TiO_2 powder with 0.5, 0.1 and 1.0%wt. was 123.7, 118.1 and 117.4 m^2/g, respectively. The highest amount of adsorbed dye contained 0.5%wt. NiO/TiO_2. The decreasing amount of adsorbed dye at 0.1 and 1.0%wt. was obtained because of dye on photoanode

cannot dissolved in solution and metal oxide cling not good on anode electrode. Accordingly, there was a diffused limitation of the dye molecule. [48]

Table 5.11 The concentration of N3 dye contained in the NiO/TiO_2 electrode at various content of NiO

Sample	Concentration of N3 dye ($\times 10^7$ mol/cm^2)
Pure TiO_2	1.39±0.003
0.1%wt. NiO/TiO_2	3.15±0.004
0.5%wt. NiO/TiO_2	3.40±0.006
1.0%wt. NiO/TiO_2	1.93±0.037
3.0%wt. NiO/TiO_2	1.75±0.002

The addition of NiO is shown to be effective at reducing recombination losses to the redox electrolyte but is found to be unable to retard recombination dynamics to the dye cation sufficiently to allow efficient dye regeneration without resulting in concomitant losses of electron injection efficiency. (see Figure 5.6)

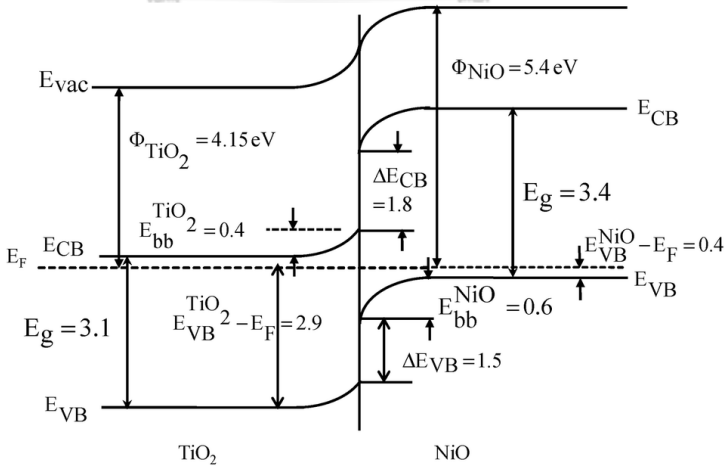

Figure 5.6 Band alignment at the heterojunction interface of n-type (TiO_2) and p-type (NiO) semiconductors. [49]

The current-voltage (I-V) characteristics of DSSCs were shown in Table 5.12. On the other hand, enhancement in short-current density (J_{sc}) is attributed to dye adsorption as the increasing of the specific surface area and increasing of dye loading capacity are strongly influenced by the electrostatic and interfacial chemical interactions. Due to the highest amount of adsorbed N3 dye and the highest of specific surface area, the highest cell efficiency of 5.15±0.07% was obtain with 0.5%wt. NiO/TiO_2.

Table 5.12 Electrochemical properties of DSSCs with NiO/TiO_2 electrode coated with N3 dye and were sintered at 400°C for 2 hours

NiO/TiO_2 (%wt.)	V_{oc} (Volt)	J_{sc} (mA/cm^2)	Fill Factor	Efficiency (%)
0	0.68	6.89	0.72	3.40±0.62
0.1	0.69	8.17	0.73	3.88±0.74
0.5	0.67	9.30	0.80	5.15±0.07
1.0	0.67	6.84	0.77	3.55±0.40
3.0	0.69	6.53	0.68	3.04±0.19

5.1.3 Modification of TiO_2 electrode layer by adding In_2O_3

In_2O_3/TiO_2 sols were prepared by mixing different amounts of In_2O_3 and TiO_2 sols to obtain the In_2O_3 amounts of 0.1-3.0%wt. The In_2O_3/TiO_2 sol was sprayed on the FTO glass substrates 500 times and was sintered at 400°C for two hours. In_2O_3 materials are rarely used as photoanode in dye-sensitized solar cells (DSSCs). The morphology and properties of In_2O_3 influences the overall power conversion efficiency (PCE) of the DSSCs. [50]

The XRD patterns of the samples (Figure 5.7) exhibited similar diffraction peaks, indicating that the obtained samples were the TiO_2 nanocomposite consisting major phase of anatase, a small amount of rutile and brookite. No obvious change can be observed by all appearances in any sample. At 25° showed lower anatase phase peak,

when increase In_2O_3 contents because TiO_2 sol mixed with In_2O_3 sol before calcined at 400°C. It can block the growth of the anatase crystallize size.

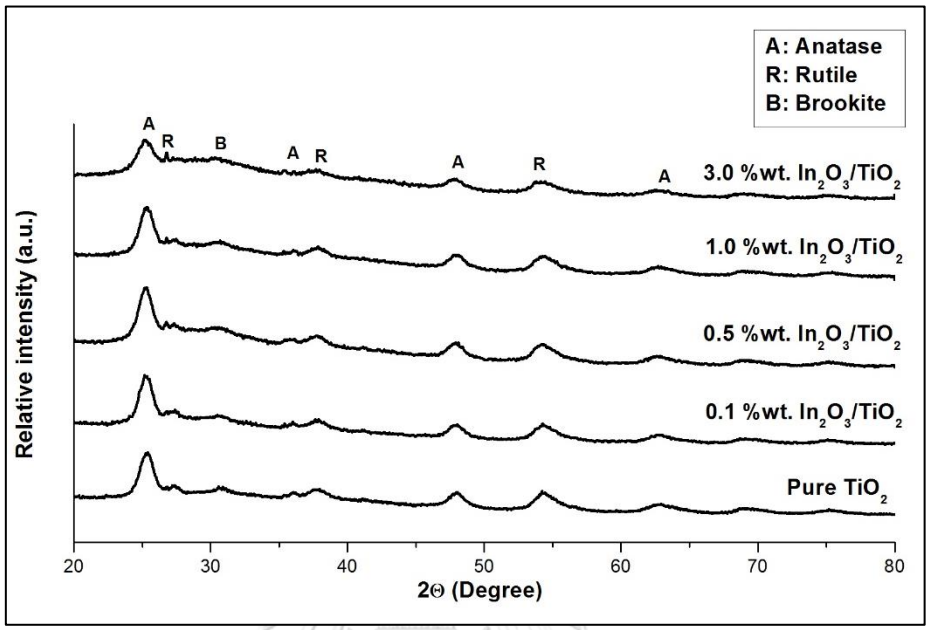

Figure 5.7 XRD patterns of In_2O_3/TiO_2 powders at various percentages of In_2O_3

Table 5.13 listed crystallite size, amount of In_2O_3 from ICP and weight fraction of TiO_2 phase in In_2O_3/TiO_2 contents. The method of the crystallite size, TiO_2 phase was presented in Appendix A, and Appendix B, respectively. The size of pure TiO_2 was 8.3 nm and the higher percentages by weight of In_2O_3/TiO_2, ranging from 0.1 to 3.0%wt. presented lower crystallite size than pure TiO_2. The growth crystallite size of anatase phase of TiO_2 was involved in the agglomeration of domain structure at the grain boundaries whereas, in the case of the modified with In_2O_3, this coalescence of structure region is restricted due to the insertion of indium atom [37].

The ICP-AES results of indium revealed that indium was presented in the In_2O_3/TiO_2 (see Table 5.13). The amount of In_2O_3 were close to the exact value. The discrepancy of In_2O_3 content was a result of preparation of mixed metal oxide sol or digestion for ICP-AES analysis.

Table 5.13 Crystallite size, surface area and weight fraction of anatase, rutile and brookite of In_2O_3/TiO_2 powder calcined at 400°C for 2 hours

Sample	Crystallite size (nm)	Amount of In_2O_3 from ICP (%wt.)	W_A	W_R	W_B
Pure TiO_2	8.3	-	0.73	0.23	0.03
0.1%wt. In_2O_3/TiO_2	7.8	0.06	0.65	0.26	0.09
0.5%wt. In_2O_3/TiO_2	7.3	0.40	0.66	0.31	0.03
1.0%wt. In_2O_3/TiO_2	7.7	0.84	0.57	0.35	0.08
3.0%wt. In_2O_3/TiO_2	7.8	2.37	0.62	0.34	0.04

Specific surface area and pore properties of In_2O_3/TiO_2 powder were determined by N_2 physisorption. (as shown in Table 5.14). Modification of TiO_2 with In_2O_3 increased specific surface area. However, the Pore volume and the pore diameter of In_2O_3/TiO_2 content differed slightly. Due to the adding lower amount of In_2O_3 when compared amount of pure TiO_2.

Table 5.14 Specific surface area, pore volume, and average pore diameter of TiO_2 and NiO/TiO_2 that were calcined at 400°C for 2 hours

Sample	BET Surface area (m^2/g)	BJH Pore volume (cm^3/g)	BJH Pore diameter (nm)
Pure TiO_2	112.8	0.196	4.90
0.1%wt. In_2O_3/TiO_2	114.4	0.255	5.02
0.5%wt. In_2O_3/TiO_2	116.0	0.247	4.97
1.0%wt. In_2O_3/TiO_2	118.8	0.245	4.96
3.0%wt. In_2O_3/TiO_2	112.9	0.249	4.92

Brennan et al. [51] reported band gap narrowing is caused by O states from In_2O_3 being introduced to the valence band region and both O and In states from In_2O_3 introduced to the conduction band (CB) region. The sub-CB states may provide

additional pathways for recombination. In_2O_3 is a wide band gap material that can be used in DSSCs as a photoanode layer. It has a direct band gap of 3.60 eV [52]. However, the addition of In_2O_3 widened the band gap was increased. (presented on Figure 5.8 and Table 5.13).

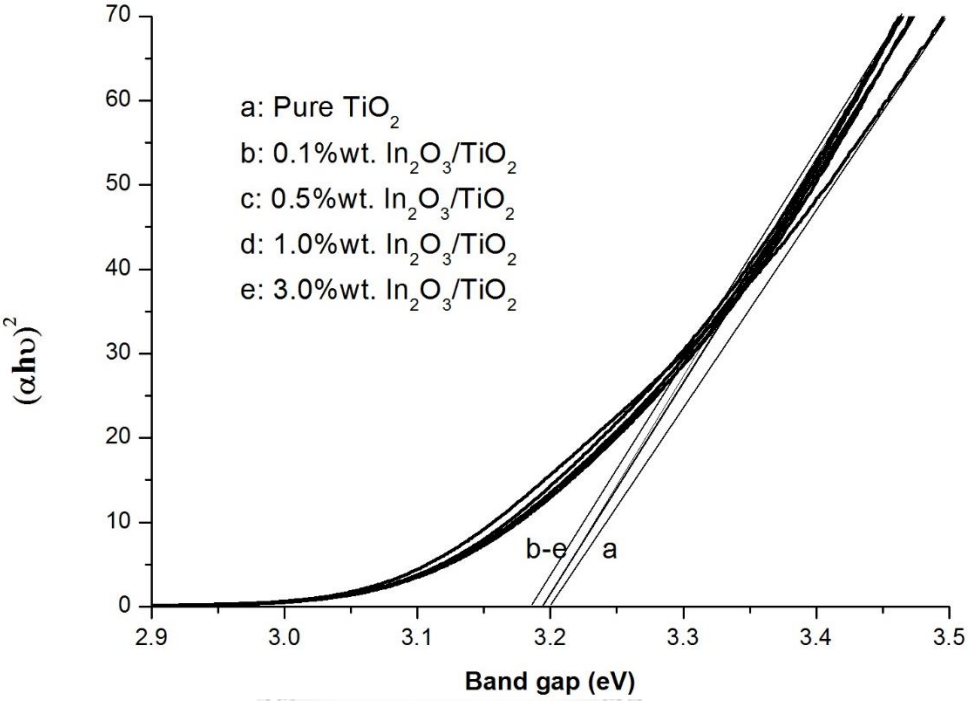

Figure 5.8 UV-visible adsorption characteristic of In_2O_3/TiO_2

Table 5.15 Band gap energy of TiO_2 and In_2O_3/TiO_2 that were calcined at 400°C for 2 hours

Sample	Wavelength (nm)	Band gap energy (eV)
Pure TiO_2	388	3.20
0.1%wt. In_2O_3/TiO_2	389	3.19
0.5%wt. In_2O_3/TiO_2	389	3.19
1.0%wt. In_2O_3/TiO_2	388	3.20
3.0%wt. In_2O_3/TiO_2	390	3.18

Due to the spray-coating process, the distribution of the mix metal oxide on photoanode electrode is good. The concentration of N3 dye adsorbed increased when the content of In_2O_3 on TiO_2 electrode increased to 1.0%wt. and decreased at 3.0%wt. that accorded to specific surface area at Table 5.16. Consequently, it can be concluded that the concentration of adsorbed N3 dye corresponded to surface area of semiconductor.

Table 5.16 The concentration of N3 dye contained in In_2O_3/TiO_2 electrode at various content of In_2O_3

Sample	Concentration of N3 dye ($\times 10^7$ mol/cm^2)
Pure TiO_2	1.39±0.003
0.1%wt. In_2O_3/TiO_2	2.20±0.020
0.5%wt. In_2O_3/TiO_2	2.78±0.007
1.0%wt. In_2O_3/TiO_2	2.85±0.003
3.0%wt. In_2O_3/TiO_2	2.37±0.010

The conduction band (CB) of TiO_2 moves downward gradually with increasing the In_2O_3 content. Dye-sensitized solar cells based on the In_2O_3-doped TiO_2 show an advantage in repressing the charge recombination. The electron lifetime in the DSSC is significantly improved by the In_2O_3-doping. As a result of the positive shift of the CB and repressed charge recombination, the short circuit photocurrent (J_{sc}) of the DSSC is improved remarkably. The collective effect of the positive shift of the CB and the enhanced electron lifetime caused by the W-doping makes the open-circuit photo-voltage (V_{oc}) remain almost unchanged. (see Figure 5.9)

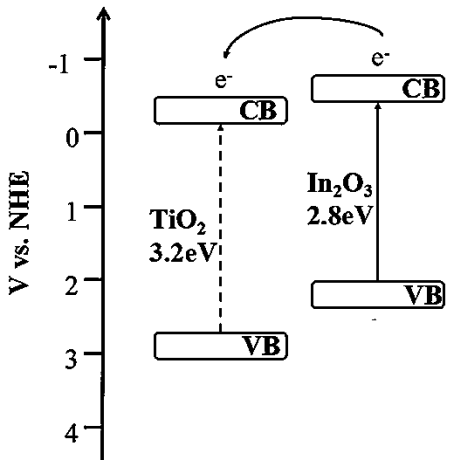

Figure 5.9 Mechanism schematic for the excitation of TiO_2–In_2O_3 under visible light irradiation. [53]

It was clear that higher open-circuit voltage (V_{oc}) could be attributed to fewer electron-hole recombination and higher current density (J_{sc}) suggested more electrons that were produced from a light harvest process and injection into conduction band. The large J_{sc} is due to the injected electrons which are forced to drive a large force with a great energy gap between conductive band and lowest unoccupied molecular orbital of dye. In Table 5.15, increasing the content of In_2O_3 increased the DSSC efficiency and was seen by the increase in the current density (J_{sc}) [54]. While, the differed only slightly V_{oc} is because In_2O_3 has more positive potentials. Thus, the 1.0%wt. In_2O_3/TiO_2 electrode showed the best photovoltaic performance, with the short-circuit photocurrent density (J_{sc}), open-circuit voltage (V_{oc}) and fill factor (FF) of 11.62 mA/cm^2, 0.70 V and 0.76, respectively, yielding an overall conversion efficiency of 6.21±0.87%.

Table 5.17 Electrochemical properties of DSSCs with In_2O_3/TiO_2 electrode coated with N3 dye and were sintered at 400°C for 2 hours

In_2O_3/TiO_2 (%wt.)	V_{oc} (Volt)	J_{sc} (mA/cm^2)	Fill Factor	Efficiency (%)
0	0.68	6.89	0.72	3.40±0.62
0.1	0.67	6.41	0.66	2.82±0.09
0.5	0.67	11.44	0.64	4.87±0.54
1.0	0.70	11.62	0.76	6.21±0.87
3.0	0.72	5.32	0.63	2.45±0.66

5.2 Modification of DSSCs using double-layered structure

A new strategy for enhancing the efficiency of TiO_2 dye-sensitized solar cells (DSSCs) by design of a new double-layer film doped with 1.0%wt. In_2O_3/TiO_2. Fabrication of a light scattering layer is an effective method for enhancing the light harvesting capacity of DSSCs, which increases an equivalent optical path and thereby enhances a photocurrent density [55]. We prepared a double-layer for DSSC device TiO_2 or second metal oxide/TiO_2 by a sol-gel method. The specific surface area of TiO_2 or second metal oxide/TiO_2 must be similar. A TiO_2 or second metal oxide/TiO_2 sol was coated using an ultrasonic spray coater on FTO glass and sintered at 400°C for two hours. In order to examine light scattering effect, we have employed different three structure as following these;

Structure (a): Single-layer structure of 1.0%wt. In_2O_3/TiO_2 from section 5.1.3

The 1.0%wt. In_2O_3/TiO_2 electrode showed the best photovoltaic performance, yielding an overall conversion efficiency of 6.21±0.87% for single-layer structure. The number of layers of 1.0%wt. In_2O_3/TiO_2 was 500 coats. An electrode was sintered at 400°C for two hours.

Structure (b): Double-layer structure type I

A double-layered structure was employed with pure TiO_2 for under-layer film that coated using an ultrasonic spray coater on FTO glass 250 times and sintered at 400°C for two hours after that, we coated 1.0%wt. In_2O_3/TiO_2 for over-layer on FTO glass 250 times and sintered at 400°C for 30 minutes.

Structure (c): Double-layer structure type II

A double-layered structure was employed with 1.0%wt. In_2O_3/TiO_2 for under-layer film that coated using an ultrasonic spray coater on FTO glass 250 times and sintered at 400°C for two hours after that, we coated pure TiO_2 for over-layer on FTO glass 250 times and sintered at 400°C for 30 minutes.

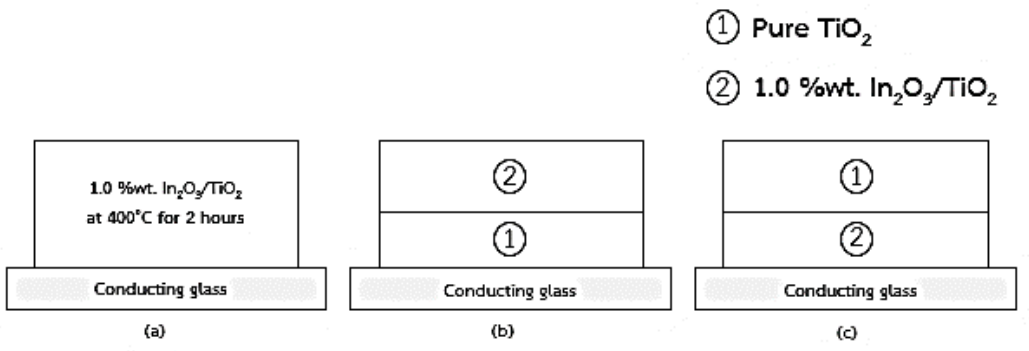

Figure 5.10 Structures of DSSC, (a) Single-layer structure (b) Double-layered structure type I and (b) Double-layered structure type II

After that, prior to N3 dye immersion, an electrode was gradually heated to 110°C and was held for 10 minutes to remove water. Then the electrode was slowly slid into a solution of N3 dye for 20-24 hours in the dark. Finally, the electrode was washed with ethanol to remove excess dye and was dried with a blow dryer. Table 5.16 showed the crystallite size, specific surface area and concentration of adsorption dye on photoanode electrode. For Single-layer structure electrode, the crystallize size of 1.0%wt. In_2O_3/TiO_2 was 7.7 nm. Whereas, Double-layered structure (Type I) electrode 6.4 nm of 1.0%wt. In_2O_3/TiO_2 for over-layer and 8.1 nm of pure TiO_2 for under-layer while double-layered structure (Type II) electrode 7.9 nm of pure TiO_2 for over-layer

and 7.7 nm of 1.0%wt. In_2O_3/TiO_2 for under-layer. The specific surface area of single structure electrode was 118.8 m^2/g. The specific surface area of double-layered structure electrode for type I was (117.9+135.2)/2 = 126.6 m^2/g and Type II was (111.5+157.8)/2 = 134.6 m^2/g. The amount of adsorption N3 dye on photoanode electrode dissolved from pores in semiconductors. The highest amount of adsorbed dye contained on double-layered structure electrode Type I.

Table 5.18 The properties of single-layer and double-layer structure calcined at various temperature

Structure	Sintering step	Crystallite size (nm)	BET surface area (m^2/g)		Concentration of N3 dye ($\times 10^7$ mol/cm^2)
(a) Single-layer:					
1.0%wt. In_2O_3/TiO_2	400°C 2 hours	7.7	118.8		2.85±0.003
(b) Double-layer type I:					
Pure TiO_2 (under-layer)	400°C 2 hours + 30 min	8.1	117.9	126.6	2.96±0.012
1.0%wt. In_2O_3/TiO_2 (over-layer)	400°C 30 min	6.4	135.2		
(c) Double-layer type II:					
1.0%wt. In_2O_3/TiO_2 (under-layer)	400°C 2 hours + 30 min	7.7	111.5	134.6	2.89±0.008
Pure TiO_2 (over-layer)	400°C 30 min	7.9	157.8		

The prior challenge in improving the properties of TiO_2 is to shift the absorption spectrum of TiO_2 towards the visible region for efficient solar light photons harvesting. The band gap was slightly widened to 3.00-3.13 eV for all sample (presented in Table 5.19)

Table 5.19 Band gap energy of TiO_2 and 1.0%wt.In_2O_3/TiO_2 that were calcined at various temperature

Structure	Sintering step	Wavelength (nm)	Band gap energy (eV)
(a) Single-layer:			
1.0%wt. In_2O_3/TiO_2	400°C 2 hr	412	3.01
(b) Double-layer type I:			
Pure TiO_2 (under-layer)	400°C 2 hours + 30 min	418	2.97
1.0%wt. In_2O_3/TiO_2 (over-layer)	400°C 30 min	416	2.98
(c) Double-layer type II:			
1.0%wt. In_2O_3/TiO_2 (under-layer)	400°C 2 hours + 30 min	418	2.97
Pure TiO_2 (over-layer)	400°C 30 min	417	2.97

The comparison of reflection spectra of three structure shown in Figure 5.11. The light scattering of over-layer enhances harvesting light of the DSSCs and the under-layer ensures good electronic contact between film electrode and the Fluorine-doped tin oxide (FTO) glass substrate. It can imply that double-layered electrode has to improve diffused reflection range of 400-800 nm compared with the single-layer electrode. Type I electrode shows the highest reflectance in the wavelength range of 400-800 nm.

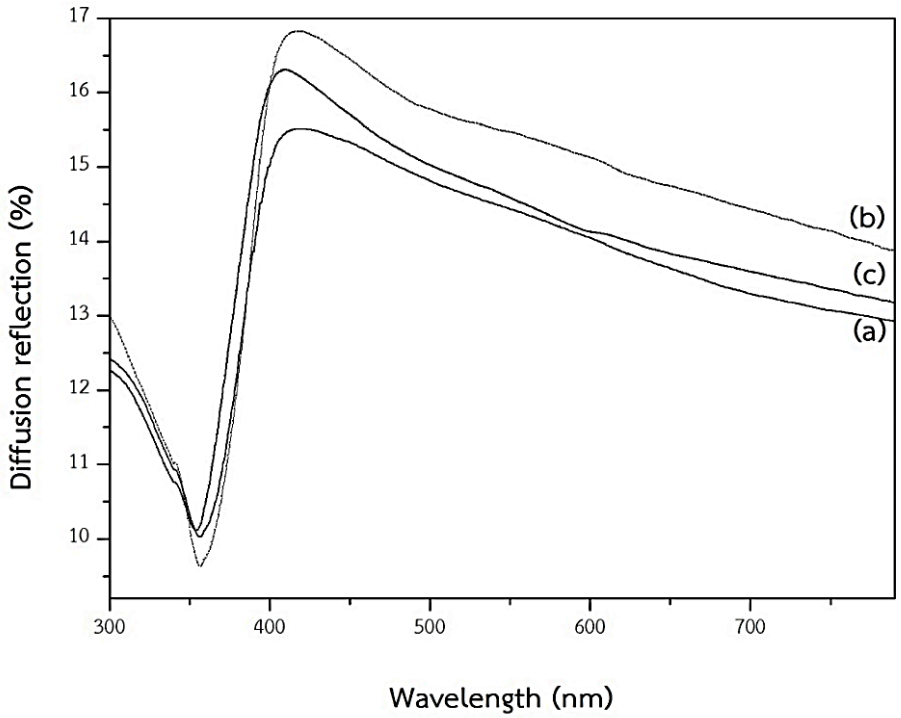

Figure 5.11 Different reflection of DSSC, (a) Single-layer structure (b) Double-layered structure Type I, and (c) Double-layered structure Type II

Dye-sensitized solar cells based on double-layered composite films (namely Type I) of Pure TiO_2 (under-layer) and 1.0%wt. In_2O_3/TiO_2 (over-layer) exhibit the highest photo-electric conversion efficiency mainly due to the combined effect of two factors, the high light scattering of over-layer 1.0%wt. In_2O_3/TiO_2 that enhance harvesting light of the dye-sensitized solar cells and the Pure TiO_2 (under-layer) that ensures good electronic contact between the TiO_2 film and FTO conducting glass. The double-layered composite film electrodes are a promising development in enhancing the performance of dye-sensitized solar cells.

This double-layer structure photoanode can offer excellent light harvesting due to longer wavelength absorption and better electron-transport properties. However, this scattering layer cannot enhance the surface area adequately to improve the dye adsorption and also it increases the thickness of photoanode due to which interfacial resistances are increased. The most applicable approach to this dilemma is to produce

a new structure having both properties of appropriate light scattering and higher surface area, and this could be achieved by making a composite structure of small and large particles in an optimal proportion. [56]

The electrochemical properties of single-layer and double-layer structure of DSSC (see Table 5.18). The photovoltaic properties were measured in the same condition as mentioned in single-layer cell. The open-circuit voltage (V_{oc}) none differed from single-layer cell. Short-circuit photocurrent density (J_{sc}) vastly increased from 11.62 to 13.71 mA/cm^2 when using of light scattering layer. Furthermore, the high surface areas of sample is respectively beneficial to adsorption of dye molecules and transfer of electrolyte solution.

The efficiency amazingly enhanced from 6.21±0.87% for single-layered structure to 7.95±0.40% for double-layer structure namely Type I.

Table 5.20 Electrochemical properties of single-layer and double-layer structure of DSSC

Structure	V_{oc} (Volt)	J_{sc} (mA/cm^2)	Fill Factor	Efficiency (%)
(a) Single-layer:				
1.0%wt. In_2O_3/TiO_2	0.70	11.62	0.76	6.21±0.87
(b) Double-layer:				
Pure TiO_2 (under-layer)	0.69	13.71	0.84	7.95±0.40
1.0%wt. In_2O_3/TiO_2 (over-layer)				
(c) Double-layer:				
1.0%wt. In_2O_3/TiO_2 (under-layer)	0.67	13.12	0.82	7.18±0.34
Pure TiO_2 (over-layer)				

CHAPTER 6
CONCLUSION AND RECOMMENDATIONS

In summary, DSSCs have been successfully prepared from CuO, NiO, or In_2O_3 coating on TiO_2 by a sol-gel method. The double-layered structured have been also investigated in this research. Thus, we divided conclusion in two part: First, presented conclusion for single-layered and double-layered of second metal oxide/TiO_2 electrode. Eventually, presented recommendation for the future work.

6.1 Conclusion

6.1.1 Modification of TiO_2 electrode single-layer by adding CuO

A CuO/TiO_2 interface with potential use for solar light conversion is studied. CuO/TiO_2 was successfully synthesized using sol-gel methods. Introduction of CuO caused the band gap to become narrower. When the CuO content was increased beyond 0.1%wt., the amount of N3 dye adsorbed on the electrode decreased even though the specific surface area was essentially unchanged. The highest power conversion efficiency was obtained with the DSSC assembled with 0.1%wt. CuO/TiO_2 electrode (4.03±0.58%).

6.1.2 Modification of TiO_2 electrode single-layer by adding NiO

The NiO/TiO_2 nanoparticles have been successfully synthesized. The band gap energy of NiO/TiO_2 was slightly widened to the visible region of the absorption edge reveals that good contact between NiO and TiO_2 in consequence of inter-dispersion of the two oxides. NiO was improving photocurrent by increasing dye absorption, increasing surface area and suppressing electron–hole recombination. The highest power conversion efficiency was 5.15±0.07% obtain by 0.5%wt. NiO.

6.1.3 Modification of TiO_2 electrode single-layer by adding In_2O_3

Indium oxide (In_2O_3) on TiO_2 thin films were prepared by sol-gel method via spray coating technique for dye-sensitized solar cells (DSSCs). The In_2O_3/TiO_2 have

successfully investigated the influence of DSSCs. Small increasing band gap value assisted at lowering in chance of electrons-holes recombination. The crystallite size of the nanoparticles decreased as the amount of In_2O_3 was added in the TiO_2 nanocomposite. Moreover, incorporation of In_2O_3/TiO_2 increased the surface area. As a result, increasing dye absorption on photoanode electrode. The 1.0%wt. exhibited highest power conversion efficiency of 6.21±0.87%.

6.1.4 Modification of DSSCs using double-layered structure

Double-layered structure electrodes not only have high specific surface areas, but also exhibit high light-scattering ability and good photo-electric conversion efficiency. DSSCs based on double-layered composite films of 1.0%wt. In_2O_3 and pure TiO_2 exhibit the highest photo-electric conversion efficiencies mainly due to the combined effect of two factors, the high light scattering of over-layer 1.0%wt. In_2O_3 enhancing harvesting light of the DSSCs and the under-layer pure TiO_2 layer ensuring good electronic contact between film electrode and conducting substrate. The efficiency was heighten from 6.21±0.87% (Type I) to 7.95±0.40% when compared with single-layer of 1.0%wt. In_2O_3/TiO_2.

6.2 Recommendation for the future work

1. Improve the efficiency of DSSC with other metal oxide
2. Using another method to preparation of photoanode electrode compared to the convectional sol-gel method.
3. Using other material for coating for counter electrode replace platinum film.
4. Immersing electrode with other Ruthenium-based or Natural dyes compared to the Ruthenium-based N3 dye.
5. Changing the electrolyte replace I_3^-/I^- redox couple.

REFERENCES

[1] Ye, M.; Wen, X.; Wang, M.; Iocozzia, J.; Zhang, N.; Lin, C.; Lin, Z., Recent advances in dye-sensitized solar cells: from photoanodes, sensitizers and electrolytes to counter electrodes. *Materials Today* **2015,** *18* (3), 155-162.

[2] Toster, J.; Iyer, K. S.; Xiang, W.; Rosei, F.; Spiccia, L.; Raston, C. L., Diatom frustules as light traps enhance DSSC efficiency. *Nanoscale* **2013,** *5* (3), 873-6.

[3] Sauvage, F.; Decoppet, J. D.; Zhang, M.; Zakeeruddin, S. M.; Comte, P.; Nazeeruddin, M.; Wang, P.; Gratzel, M., Effect of sensitizer adsorption temperature on the performance of dye-sensitized solar cells. *J Am Chem Soc* **2011,** *133* (24), 9304-10.

[4] O'Regan, B.; Grätzel, M., A low-cost, high-efficiency solar cell based on dye-sensitized colloidal TiO_2 films. *Nature* **1991,** *353*, 737-740.

[5] Youngblood, W. J.; Seung-Hyun Anna Lee; Kobayashi, Y.; Hernandez-Pagan, E. A.; Hoertz, P. G.; Moore, T. A.; Moore, A. L.; Gust, D.; Mallouk, T. E., Photoassisted Overall Water Splitting in a Visible Light-Absorbing Dye-Sensitized Photoelectrochemical Cell. *Am. Chem. Soc.* **2009,** *131* (3), 926–927.

[6] Hagfeldt, A.; Boschloo, G.; Sun, L.; Kloo, L.; Pettersson, H., Dye-Sensitized Solar Cells. *Chem. Rev.* **2010,** *110* (11), 6595–6663.

[7] Grätzel, M., Dye-sensitized solar cells. *Journal of Photochemistry and Photobiology C: Photochemistry Reviews* **2003,** *4* (2), 145-153.

[8] Dahlan, D.; Md Saad, S. K.; Berli, A. U.; Bajili, A.; Umar, A. A., Synthesis of two-dimensional nanowall of Cu-Doped TiO_2 and its application as photoanode in DSSCs. *Physica E: Low-dimensional Systems and Nanostructures* **2017,** *91*, 185-189.

[9] Susanti, D.; Nafi, M.; Purwaningsih, H.; Fajarin, R.; Kusuma, G. E., The Preparation of Dye Sensitized Solar Cell (DSSC) from TiO_2 and Tamarillo Extract. *Procedia Chemistry* **2014,** *9*, 3-10.

[10] Ko, K. H.; Lee, Y. C.; Jung, Y. J., Enhanced efficiency of dye-sensitized TiO_2 solar cells (DSSC) by doping of metal ions. *J Colloid Interface Sci* **2005,** *283* (2), 482-7.

[11] Wang, H.-H.; Su, C.; Chen, H.-S.; Liu, Y.-C.; Hsu, Y.-W.; Hsu, N.-M.; Li, W.-R., Preparation of Nanoporous TiO_2 Electrodes for Dye-Sensitized Solar Cells. *Journal of Nanomaterials* **2011,** *2011*, 1-7.

[12] GB, S.; JK, L.; FS, L.; TJ, P.; GH, R., Preparation and phase transformation of anatase–rutile crystals in metal doped TiO_2/muscovite nanocomposites. *Thin Solid Films* **2005,** *491*, 110-16.

[13] Na-Phattalung, S.; Smith, M. F.; Kim, K.; Du, M.-H.; Wei, S.-H.; Zhang, S. B.; Limpijumnong, S., First-principles study of native defects in anatase TiO_2. *Physical Review B* **2006,** *73* (12).

[14] Ghanbari Niaki, A. H.; Bakhshayesh, A. M.; Mohammadi, M. R., Double-layer dye-sensitized solar cells based on Zn-doped TiO_2 transparent and light scattering layers: Improving electron injection and light scattering effect. *Solar Energy* **2014,** *103*, 210-222.

[15] Karthikeyan, C. S.; Thelakkat, M.; Willert-Porada, M., Different mesoporous titania films for solid-state dye sensitised solar cells. *Thin Solid Films* **2006,** *511-512*, 187-194.

[16] Li, B.; Wang, X.; Yan, M.; Li, L., Preparation and characterization of nano-TiO_2 powder. *Materials Chemistry and Physics* **2002,** (78), 184–188.

[17] Valencia, S.; Vargas, X.; Rios, L.; Restrepo, G.; Marín, J. M., Sol–gel and low-temperature solvothermal synthesis of photoactive nano-titanium dioxide. *Journal of Photochemistry and Photobiology A: Chemistry* **2013,** *251*, 175-181.

[18] Wang, Y. X.; Xu, M.; Sun, J., Preparation of TiO_2 Nanopowders by Non-Hydrolytic Sol–Gel and Solvothermal Synthesis. *Applied Mechanics and Materials* **2011,** *110-116*, 1934-1939.

[19] O.Harizanov; A.Harizanova, Development and investigation of sol–gel solutions for the formation of TiO_2 coatings. *Solar Energy Materials and Solar Cells* **2000,** *63* (2), 185-195.

[20] Thomas, S.; Deepak, T. G.; Anjusree, G. S.; Arun, T. A.; Nair, S. V.; Nair, A. S., A review on counter electrode materials in dye-sensitized solar cells. *J. Mater. Chem. A* **2014,** *2* (13), 4474-4490.

[21] Kay, A.; Rodicio, I.; Humphry-Baker, R.; Mueller, E.; Liska, P.; Vlachopoulos, N.; Graetzel, M.; Nazeeruddin, M. K., Conversion of light to electricity by cis-X2bis(2,2'-bipyridyl-4,4'-dicarboxylate)ruthenium(II) charge-transfer sensitizers (X = Cl^-, Br^-, I^-, CN^-, and SCN^-) on nanocrystalline titanium dioxide electrodes. *J. Am. Chem. SOC.* **1993,** *115* (14), 6382-6390.

[22] Ryan, M., PGM HIGHLIGHTS: Progress in Ruthenium Complexes for Dye Sensitised Solar Cells. *Platinum Metals Review* **2009,** *53* (4), 216-218.

[23] Chiba, Y.; Islam, A.; Watanabe, Y.; Komiya, R.; Koide, N.; Han, L., Dye-Sensitized Solar Cells with Conversion Efficiency of 11.1%. *Japanese Journal of Applied Physics* **2006,** *45* (25), L638–L640.

[24] Nazeeruddin, M. K.; De Angelis, F.; Fantacci, S.; Selloni, A.; Viscardi, G.; Liska, P.; Ito, S.; Takeru, B.; Grätzel, M., Combined Experimental and DFT-TDDFT Computational Study of Photoelectrochemical Cell Ruthenium Sensitizers. *Chemical Society Journal of the American Chemical Society* **2005,** *127* (48), 16835-16847.

[25] Boschloo, G.; Hagfeldt, A., Characteristics of the Iodide/Triiodide Redox Mediator in Dye-Sensitized Solar Cells. *Accounts of Chemical Research* **2009,** *42* (11), 1819-1826.

[26] Wu, J.; Lan, Z.; Lin, J.; Huang, M.; Huang, Y.; Fan, L.; Luo, G.; Lin, Y.; Xie, Y.; Wei, Y., Counter electrodes in dye-sensitized solar cells. *Chem Soc Rev* **2017,** *46* (19), 5975-6023.

[27] Tayyan, A. A. E., Dye sensitized solar cell: parameters calculation and model integration. *Journal of Electron Devices* **2011,** *11*, 616-624.

[28] Dupré, O.; Vaillon, R.; Green, M. A., Temperature Coefficients of Photovoltaic Devices. **2017**, 29-74.

[29] Zhou, L.; Wei, L.; Yang, Y.; Xia, X.; Wang, P.; Yu, J.; Luan, T., Improved performance of dye sensitized solar cells using Cu-doped TiO_2 as photoanode materials: Band

edge movement study by spectroelectrochemistry. *Chemical Physics* **2016,** *475*, 1-8.

[30] Obina, W. M.; Cari; Supriyanto, A.; Sumardiasih, S.; Septiawan, T. Y.; Khairuddin, Fabrication and variation layers of Cu/TiO_2 nanocomposite and its applications in Dye-Sensitized Solar Cell (DSSC). *Journal of Physics: Conference Series* **2017,** *795*, 012029.

[31] Sahu, G.; Tarr, M. A., Improved performance of three-dimensional Ni–TiO_2 core–shell nanowire photoanodes in dye-sensitized solar cells. *MRS Communications* **2013,** *3* (04), 199-205.

[32] Sakthivel, T.; Kumar, K. A.; Senthilselvan, J.; Jagannathan, K., Effect of Ni dopant in TiO_2 matrix on its interfacial charge transportation and efficiency of DSSCs. *Journal of Materials Science: Materials in Electronics* **2017,** *29* (3), 2228-2235.

[33] Chen, Y.; Zhou, X.; Zhao, X.; He, X.; Gu, X., Crystallite structure, surface morphology and optical properties of In_2O_3–TiO_2 composite thin films by sol–gel method. *Materials Science and Engineering: B* **2008,** *151* (2), 179-186.

[34] Hwang, K.-J.; Park, D.-W.; Jin, S.; Kang, S. O.; Cho, D. W., Influence of dye-concentration on the light-scattering effect in dye-sensitized solar cell. *Materials Chemistry and Physics* **2015,** *149-150*, 594-600.

[35] Choi, J. O.; Lee, G. Y.; Kim, C. S.; Kim, D. H.; Kim, M. S.; Chun, D. M.; Ahn, S. H., Dye-sensitised solar cell (DSSC) with TiO_2 multilayer fabricated by nano particle deposition system *18th International conference on composite materials*.

[36] Chou, C.-S.; Guo, M.-G.; Liu, K.-H.; Chen, Y.-S., Preparation of TiO_2 particles and their applications in the light scattering layer of a dye-sensitized solar cell. *Applied Energy* **2012,** *92*, 224-233.

[37] Kaur, M.; Verma, N. K., $CaCO_3$/TiO_2 Nanoparticles Based Dye Sensitized Solar Cell. *Journal of Materials Science & Technology* **2014,** *30* (4), 328-334.

[38] Arroyo, R.; Co´rdoba, G.; Padilla, J.; Lara, V. H., Influence of manganese ions on the anatase–rutile phase transition of TiO_2 prepared by the sol–gel process. *Materials Letters* **2002,** *54* (5–6), 397-402.

[39] Dette, C.; Perez-Osorio, M. A.; Kley, C. S.; Punke, P.; Patrick, C. E.; Jacobson, P.; Giustino, F.; Jung, S. J.; Kern, K., TiO_2 anatase with a bandgap in the visible region. *Nano Lett* **2014,** *14* (11), 6533-8.

[40] Park, J.-Y.; Kim, C.-S.; Okuyama, K.; Lee, H.-M.; Jang, H.-D.; Lee, S.-E.; Kim, T.-O., Copper and nitrogen doping on TiO_2 photoelectrodes and their functions in dye-sensitized solar cells. *Journal of Power Sources* **2016,** *306*, 764-771.

[41] Palomares, E.; Clifford, J. N.; Haque, S. A.; Lutz, T.; Durrant, J. R., Slow charge recombination in dye-sensitised solar cells (DSSC) using Al_2O_3 coated nanoporous TiO_2 films. *Chemical Communications* **2002,** (14), 1464-1465.

[42] Bandara, J.; Udawatta, C. P.; Rajapakse, C. S., Highly stable CuO incorporated TiO_2 catalyst for photo-catalytic hydrogen production from H_2O. *Photochem Photobiol Sci* **2005,** *4* (11), 857-61.

[43] Bakhshayesh, A. M.; Bakhshayesh, N., Improved short-circuit current density of dye-sensitized solar cells aided by Sr,Nb co-doped TiO_2 spherical particles derived from sol–gel route. *Journal of Sol-Gel Science and Technology* **2015,** *77* (1), 228-239.

[44] Futemvong, S.; Pengpad, A.; Hongsith, N.; Wongratanaphisan, D.; Gardchareon, A.; Choopun, S., Effect of Nickel Oxide Thin Films on Photoconversion Efficiency in Zinc Oxide Dye-Sensitized Solar Cells. *Materials Science Forum* **2011,** *695*, 509-512.

[45] Bandara, J., Corrigendum to Fabrication of n-p junction electrodes made of n-type SnO_2 and p-type NiO for control of charge recombination in dye-sensitized solar cells *Solar Energy Materials and Solar Cells* **2004,** *81* (4), 4290-4379.

[46] Song, G. B.; Liang, J. K.; Liu, F. S.; Peng, T. J.; Rao, G. H., Preparation and phase transformation of anatase–rutile crystals in metal doped TiO_2/muscovite nanocomposites. *Thin Solid Films* **2005,** *491* (1-2), 110-116.

[47] Ku, Y.; Lin, C.-N.; Hou, W.-M., Characterization of coupled NiO/TiO_2 photocatalyst for the photocatalytic reduction of Cr(VI) in aqueous solution. *Journal of Molecular Catalysis A: Chemical* **2011,** *349* (1-2), 20-27.

[48] Lee, C.-P.; Li, C.-T.; Ho, K.-C., Use of organic materials in dye-sensitized solar cells. *Materials Today* **2017,** *20* (5), 267-283.

[49] Uddin, M. T.; Nicolas, Y.; Olivier, C.; Jaegermann, W.; Rockstroh, N.; Junge, H.; Toupance, T., Band alignment investigations of heterostructure NiO/TiO_2 nanomaterials used as efficient heterojunction earth-abundant metal oxide photocatalysts for hydrogen production. *Phys Chem Chem Phys* **2017,** *19* (29), 19279-19288.

[50] Mahalingam, S.; Abdullah, H., Electron transport study of indium oxide as photoanode in DSSCs: A review. *Renewable and Sustainable Energy Reviews* **2016,** *63*, 245-255.

[51] Brennan, T. P.; Tanskanen, J. T.; Roelofs, K. E.; To, J. W. F.; Nguyen, W. H.; Bakke, J. R.; Ding, I. K.; Hardin, B. E.; Sellinger, A.; McGehee, M. D.; Bent, S. F., TiO_2 Conduction Band Modulation with In_2O_3 Recombination Barrier Layers in Solid-State Dye-Sensitized Solar Cells. *The Journal of Physical Chemistry C* **2013,** *117* (46), 24138-24149.

[52] Raza, A.; Agnihotri, P.; Gupta, B. K., Preparation and intrinsic absorption in the band edge in chemically sprayed In_2O_3 layers. *Journal of Physics D: Applied Physics* **1977,** *10* (13).

[53] Heng, H.; Gan, Q.; Meng, P.; Liu, X., $H_3PW_{12}O_{40}/TiO_2$–In_2O_3: a visible light driven type-II heterojunction photocatalyst for the photocatalytic degradation of imidacloprid. *RSC Advances* **2016,** *6* (77), 73301-73307.

[54] Arifin, Z.; Soeparman, S.; Widhiyanuriyawan, D.; Suyitno, S., Performance Enhancement of Dye-Sensitized Solar Cells Using a Natural Sensitizer. *International Journal of Photoenergy* **2017,** *2017*, 1-5.

[55] Park, J. T.; Roh, D. K.; Chi, W. S.; Patel, R.; Kim, J. H., Fabrication of double layer photoelectrodes using hierarchical TiO_2 nanospheres for dye-sensitized solar cells. *Journal of Industrial and Engineering Chemistry* **2012,** *18* (1), 449-455.

[56] Qadir, M. B.; Sun, K. C.; Sahito, I. A.; Arbab, A. A.; Choi, B. J.; Yi, S. C.; Jeong, S. H., Composite multi-functional over layer: A novel design to improve the photovoltaic performance of DSSC. *Solar Energy Materials and Solar Cells* **2015,** *140*, 141-149.

[57] Ingham, B.; Toney, M. F., X-ray diffraction for characterizing metallic films. **2014**, 3-38.

APPENDIX

APPENDIX A
CALCULATION OF THE CRYSTALLITE SIZE

Calculation of the crystallite size by Debye-Scherrer equation

The crystallite size can be calculated from 2Θ profile analysis, FWHM, by Debye-Scherrer equation that was suitable for partical size below 100 nm. [57]

Scherrer equation:

$$D = \frac{k\lambda}{\beta \cos\theta} \qquad \text{(A.1)}$$

Where

D	=	Crystallite size (Å)
k	=	Crystallite-shape factor (0.9)
λ	=	X-ray wavelength (1.5418 Å for $CuK\alpha$)
θ	=	Observed peak angel (degree)
β	=	X-ray diffraction broadening (radian)

The X-ray diffraction broadening is the pure width of the diffraction free of all broadening due to the experimental equipment. Standard λ-alumina is used to observe the instrumental broadening since its crystallite size is larger than 2000 Å. The X-ray diffraction broadening can be obtained by using Warren's equation.

Warren's equation:

$$\beta^2 = \beta_M^2 - \beta_S^2$$
$$\beta = \sqrt{\beta_M^2 - \beta_S^2} \qquad \text{(A.2)}$$

Where

β_M = Measured peak width in radians at half peak height

β_S = Corresponding width of a standard material

Example: Calculation of the crystallite site of pure TiO_2 sintered at 400°C for two hours

The half-weight width (101) diffraction peak = 0.986765 °

= 0.017214 radian

The corresponding half-height width of peak of TiO_2 = 0.003836 radian

The pure width = $\sqrt{\beta_M^2 - \beta_S^2}$

= $\sqrt{0.017214^{\ 2} - 0.003836^{\ 2}}$

= 0.0168 radian

Where

β = 0.0168 radian

2θ = 25.345 °

θ = 12.672 °

λ = 1.5418 Å

The crystallite size = $\frac{0.9 \times 1.5418}{0.0168 \cos(12.672)}$ = 83.16 Å = 8.32 nm

APPENDIX F

CALCULATION OF WEIGHT FRACTION OF ANATASE, RUTILE AND BROOKITE PHASE OF TiO_2

The phase of TiO_2 can be detected at 2Θ of 25.3°, 37.2°, 48.2°, and 62.8° were assigned to anatase TiO_2, whereas the peak at 27.4°, 41.3°, and 54.4° corresponded to be rutile phase and the peak at 30.9° was associated to brookite.

The weight fraction of TiO_2 sample can be calculated as follows equation (B.1)-(B.3).

$$W_A = \frac{\sum A_A}{\sum A_A + \sum A_R + \sum A_B} \quad \text{(B.1)}$$

$$W_R = \frac{\sum A_R}{\sum A_A + \sum A_R + \sum A_B} \quad \text{(B.2)}$$

$$W_B = \frac{\sum A_B}{\sum A_A + \sum A_R + \sum A_B} \quad \text{(B.3)}$$

When

W_A = Weight fraction of anatase phase TiO_2

W_R = Weight fraction of rutile phase TiO_2

W_B = Weight fraction of brookite phase TiO_2

$\sum A_A$ = Summary of the intensity of the anatase peak

$\sum A_R$ = Summary of the intensity of the rutile peak

$\sum A_B$ = Summary of the intensity of the brookite peak

Example: Calculation of the phase contents of pure TiO_2 sintered at 400°C for 2 hours

Table F.1 The integrated intensity of TiO_2 from Fityk

Phase	2Θ	Intensity	Summary intensity
Anatase	25.3°	1,076.13	2,243.00
	37.2°	210.48	
	48.2°	522.27	
	62.8°	434.15	
Rutile	27.4°	112.36	718.82
	41.3°	41.24	
	54.4°	565.22	
Brookite	30.9°	107.06	107.06

Note: Fityk is a program for data processing and nonlinear curve fitting.

$$W_A = \frac{2{,}243.00}{2{,}243.00 + 718.82 + 107.06} = 0.73$$

$$W_R = \frac{718.82}{2{,}243.00 + 718.82 + 107.06} = 0.23$$

$$W_B = \frac{107.06}{2{,}243.00 + 718.82 + 107.06} = 0.03$$

APPENDIX C

DETERMINATION OF THE AMOUNT OF RUTHENIUM-BASED DYE ADSORBED ON TITANIA SURFACE

The amount of ruthenium-based dye adsorbed was determined by UV-Visible Absorption Spectroscopy. The dye was dissolved out to surface by using a mixed solution of 0.1 M NaOH in deionized water and ethanol (1:1 volume fraction).

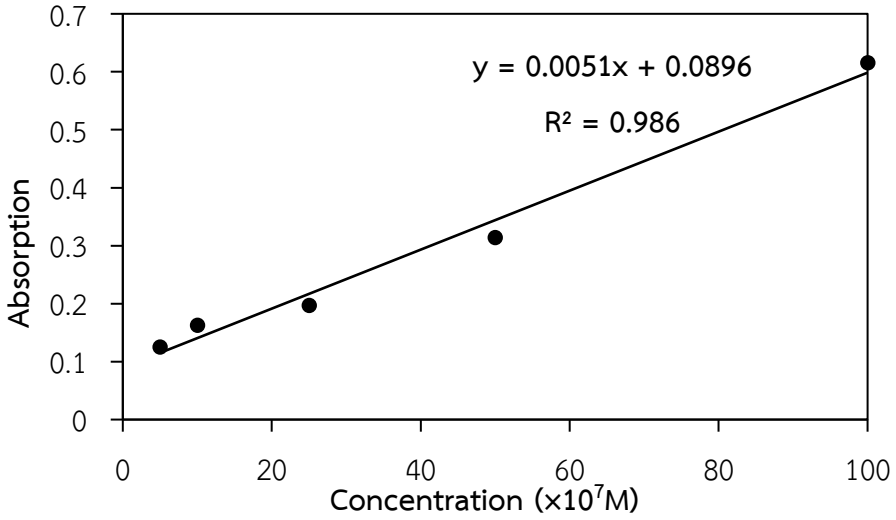

Figure C.1 The calibration curve of the concentration of N3 adsorbed dye

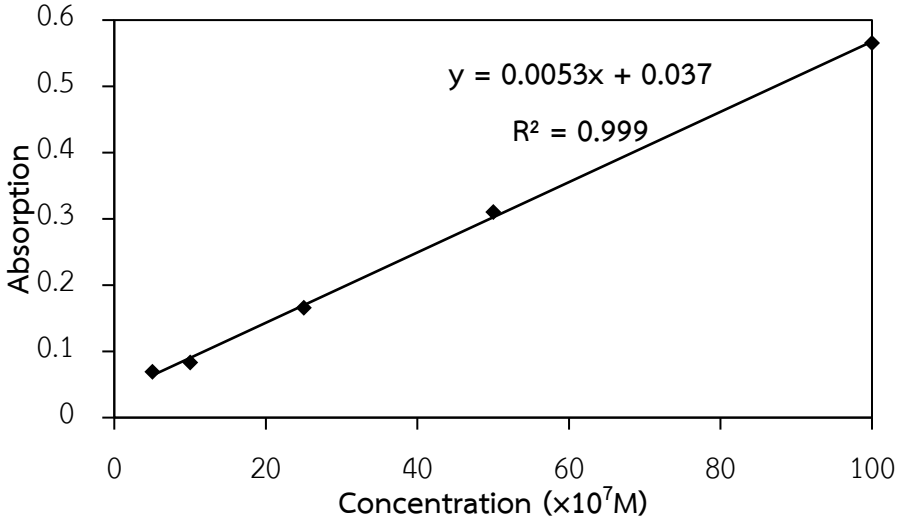

Figure C.2 The calibration curve of the concentration of N719 adsorbed dye

Table C.1 The concentration of N3 dye contained in second metal oxide/TiO_2 electrode at various content of second metal oxide

Sample	Concentration of N3 dye ($\times 10^7$ mol/cm^2)			
	1	2	3	Average
Pure TiO_2	1.32	1.43	1.41	1.39±0.003
0.1%wt. CuO/TiO_2	1.47	1.36	1.39	1.41±0.003
0.5%wt. CuO/TiO_2	1.02	0.97	1.14	1.04±0.008
1.0%wt. CuO/TiO_2	1.30	1.28	1.22	1.27±0.002
3.0%wt. CuO/TiO_2	1.15	1.26	1.20	1.20±0.003
0.1%wt. NiO/TiO_2	3.20	3.18	3.08	3.15±0.004
0.5%wt. NiO/$_3$/TiO_2	3.41	3.32	3.48	3.40±0.006
1.0%wt. NiO/TiO_2	2.07	1.71	2.01	1.93±0.037
3.0%wt. NiO/TiO_2	1.69	1.77	1.78	1.75±0.002
0.1%wt. In_2O_3/TiO_2	2.23	2.04	2.32	2.20±0.020
0.5%wt. In_2O_3/TiO_2	2.79	2.86	2.69	2.78±0.007
1.0%wt. In_2O_3/TiO_2	2.90	2.87	2.79	2.85±0.003
3.0%wt. In_2O_3/TiO_2	2.48	2.29	2.34	2.37±0.010

Table C.2 The concentration of N719 dye contained in second metal oxide/TiO_2 electrode at various content of second metal oxide

Sample	Concentration of N719 dye ($\times 10^7$ mol/cm^2)			
	1	2	3	Average
Pure TiO_2	1.60	1.43	1.53	1.52±0.007
0.1%wt. CuO/TiO_2	1.34	1.30	1.53	1.31±0.001

Sample	Concentration of N719 dye ($\times 10^7$ mol/cm^2)			
	1	2	3	Average
0.5%wt. CuO/TiO_2	0.88	0.84	1.28	0.74±0.044
1.0%wt. CuO/TiO_2	1.13	0.83	0.50	0.98±0.022
3.0%wt. CuO/TiO_2	1.14	1.09	0.98	1.07±0.006

APPENDIX D

THE CALCULATION OF THE BAND GAP ENERGY FROM UV-VIS SPECTRA

The band gap energy of the catalyst was estimated by equation (D.1)

$$E_g = \frac{hC}{\lambda} \qquad \text{(D.1)}$$

When

E_g = The band gap energy of the catalyst (eV)

h = The plank constant (6.62×10^{-34} Joules·sec)

λ = The wavelength at which the absorption begins (meters)

C = The speed of light (3.0×10^{8} meter/sec)

Note: 1 eV is 1.6×10^{-19} Joules (conversion factor)

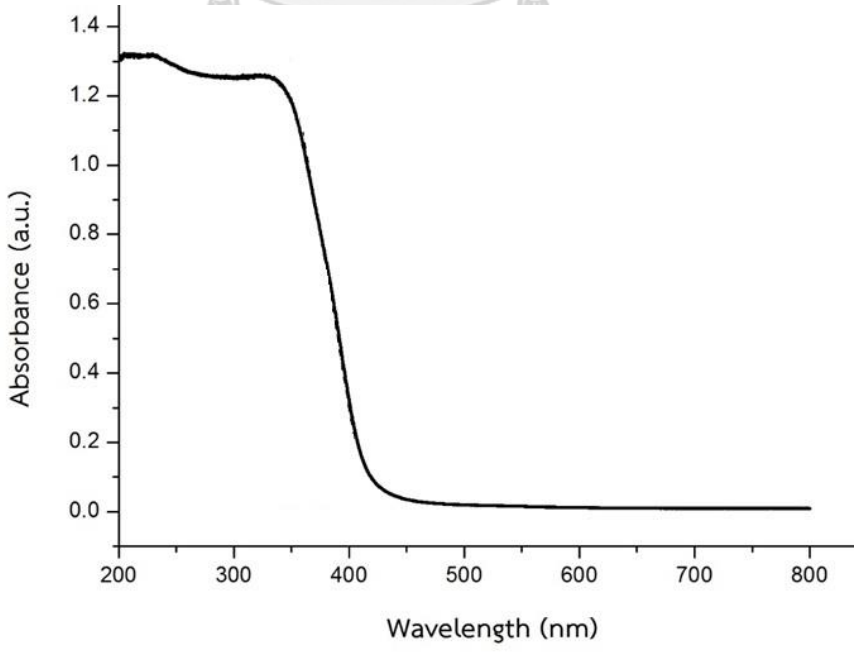

Figure D.1 UV-Visible absorption characteristics of pure TiO_2

The UV-Vis spectrum can be used to calculate the band gaps of semiconductor material, by plotting the graph between $(\alpha h\nu)^{(1/0.5)}$ versus photon energy ($h\nu$) where a: is the optical absorption coefficient, which can be calculated from absorbance (A), and thickness of the sample (t) using: (α = 2.303A/t); and ($h\nu$) can be calculated form wavelength using: ($h\nu$ = 1240/wavelength); The power factor (n = 0.5) takes the values of for allowed direct, allowed indirect, forbidden direct and forbidden indirect transition

Example: Calculation of the band gap in pure TiO_2

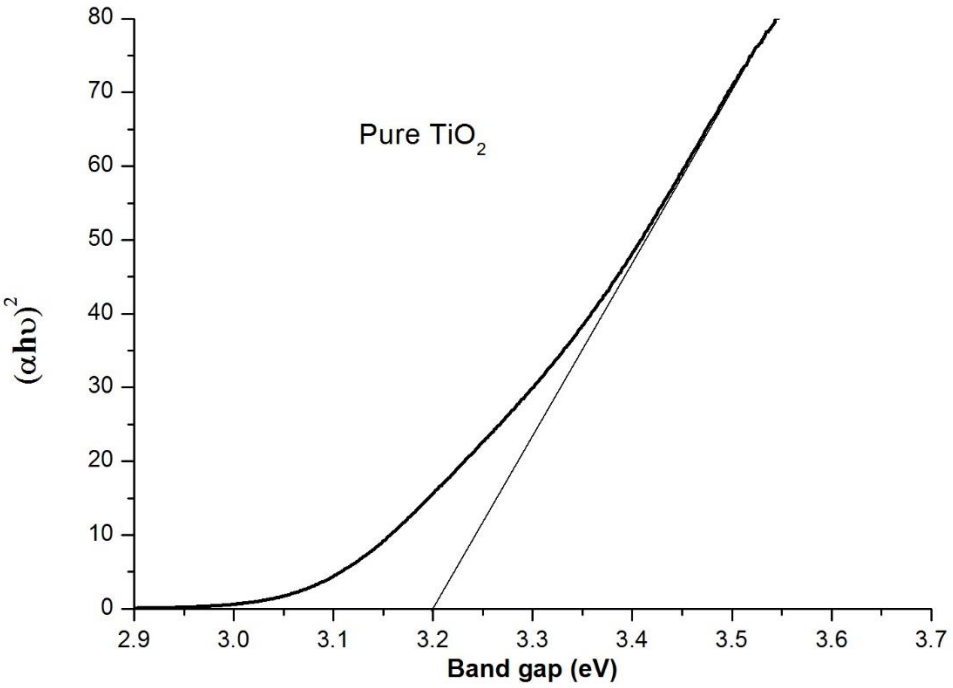

Figure D.2 The band gap of pure TiO_2

From Figure D.2 presented the band gap of pure TiO_2 is 3.20 eV

APPENDIX E

THE CALCULATION OF AMOUNT OF METAL OXIDE FROM ICP-AES

Calculation of ICP-AES results

The results from ICP-AES characterization were calculation the contents of metal oxide doped TiO_2.

Example: Calculation of the In_2O_3 contents in 1.0%wt. In_2O_3/TiO_2

For 1.0%wt. In_2O_3/TiO_2, the initial weight of catalyst powder was 0.1304 g. Hence, the calculation of Indium (In) contents as follows:

The amount of Indium oxide in catalyst were;

In 1.0 g of catalyst, had a In_2O_3 content was 0.01 g

In 0.1304 g of catalyst, had a In_2O_3 content was $\frac{0.01 \times 0.1304}{1.0}$ g

$= 1.304 \times 10^{-3}$ g

= 1.304 mg

For digestion, sample were diluted to 100 cm^3

Therefore, the sample had a concentration were $= \frac{1.304 \times 1000}{100}$

= 13.04 ppm (mg/L of In_2O_3)

From the result of ICP-AES, shown the concentration of sample 9.073 ppm

Converting to concentration of In_2O_3 = $\frac{9.073 \times 277.64}{114.82 \times 2}$

= 10.97 ppm

When

The molecular weight of Indium oxide (In_2O_3) is 277.64 g/mol

The molecular weight of Indium (In) is 114.82 g/mol

Therefore, the In_2O_3/TiO_2 contests in catalysts were calculated by

In_2O_3 concentration of 13.04 ppm refer to 1.0%wt. In_2O_3/TiO_2 in catalyst

In_2O_3 concentration of 10.97 ppm refer to $= \frac{10.97 \times 1.0}{13.04}$

$= 0.84\%wt.\ In_2O_3/TiO_2$

APPENDIX F

THE ELECTROCHEMICAL PROPERTIES OF DSSCS

Table F.1 Electrochemical properties of DSSC of pure TiO_2 electrode sintered at 400°C for 2 hours 500 coats (N3 dye)

Number of cell	V_{oc} (Volt)	J_{sc} (mA/cm^2)	Fill Factor	Efficiency (%)
1	0.75	6.64	0.70	3.49
2	0.70	7.85	0.73	4.01
3	0.59	5.79	0.74	2.53
4	0.64	6.64	0.72	3.04
5	0.72	7.56	0.72	3.92
Average	0.68	6.89	0.72	3.40±0.62

Table F.2 Electrochemical properties of DSSC of 0.1%wt. of CuO/TiO_2 electrode sintered at 400°C for 2 hours 500 coats (N3 dye)

Number of cell	V_{oc} (Volt)	J_{sc} (mA/cm^2)	Fill Factor	Efficiency (%)
1	0.68	8.11	0.75	4.09
2	0.69	7.13	0.68	3.30
3	0.67	8.37	0.75	4.19
4	0.65	9.04	0.75	4.31
5	0.69	8.29	0.74	4.24
Average	0.67	8.19	0.73	4.03±0.58

Table F.3 Electrochemical properties of DSSC of 0.5%wt. CuO/TiO_2 electrode sintered at 400°C for 2 hours 500 coats (N3 dye)

Number of cell	V_{oc} (Volt)	J_{sc} (mA/cm^2)	Fill Factor	Efficiency (%)
1	**0.70**	**5.10**	**0.65**	**2.32**
2	0.67	5.12	0.67	2.31
3	0.68	5.11	0.64	2.22
4	0.61	4.12	0.66	1.66
5	0.67	5.31	0.54	1.91
Average	0.67	4.95	0.63	2.08±0.41

Table F.4 Electrochemical properties of DSSC of 1.0%wt. CuO/TiO_2 electrode sintered at 400°C for 2 hours 500 coats (N3 dye)

Number of cell	V_{oc} (Volt)	J_{sc} (mA/cm^2)	Fill Factor	Efficiency (%)
1	0.72	3.51	0.68	1.71
2	0.60	3.42	0.67	1.37
3	0.68	4.74	0.62	1.99
4	0.69	2.74	0.53	1.00
5	0.72	3.10	0.76	1.70
Average	0.68	3.50	0.65	1.55±0.38

Table F.5 Electrochemical properties of DSSC of 3.0%wt. CuO/TiO_2 electrode sintered at 400°C for 2 hours 500 coats (N3 dye)

Number of cell	V_{oc} (Volt)	J_{sc} (mA/cm^2)	Fill Factor	Efficiency (%)
1	0.71	2.59	0.59	1.08
2	0.67	2.32	0.73	1.14
3	0.69	2.09	0.68	0.99

Number of cell	V_{oc} (Volt)	J_{sc} (mA/cm^2)	Fill Factor	Efficiency (%)
4	0.67	2.43	0.66	1.08
5	0.67	2.09	0.72	1.01
Average	0.68	2.30	0.68	1.06±0.06

Table F.6 Electrochemical properties of DSSC of pure TiO_2 electrode sintered at 400°C for 2 hours 500 coats (N719 dye)

Number of cell	V_{oc} (Volt)	J_{sc} (mA/cm^2)	Fill Factor	Efficiency (%)
1	0.74	7.03	0.64	3.31
2	0.68	5.25	0.79	2.83
3	0.70	7.66	0.68	3.68
4	0.67	7.43	0.67	3.35
5	0.69	7.43	0.65	3.35
Average	0.70	6.96	0.69	3.31±0.30

Table F.7 Electrochemical properties of DSSC of 0.1%wt. of CuO/TiO_2 electrode sintered at 400°C for 2 hours 500 coats (N719 dye)

Number of cell	V_{oc} (Volt)	J_{sc} (mA/cm^2)	Fill Factor	Efficiency (%)
1	0.72	6.57	0.75	3.52
2	0.69	6.67	0.69	3.14
3	0.69	6.89	0.75	3.55
4	0.68	6.47	0.73	3.23
5	0.69	8.35	0.63	3.64
Average	0.69	6.99	0.71	3.41±0.31

Table F.8 Electrochemical properties of DSSC of 0.5%wt. CuO/TiO_2 electrode sintered at 400°C for 2 hours 500 coats (N719 dye)

Number of cell	V_{oc} (Volt)	J_{sc} (mA/cm^2)	Fill Factor	Efficiency (%)
1	0.64	4.60	0.83	2.43
2	0.65	3.67	0.72	1.74
3	0.66	3.15	0.67	1.38
4	0.67	3.28	0.56	1.24
5	0.66	3.73	0.57	1.40
Average	0.66	3.69	0.67	1.64±0.68

Table F.9 Electrochemical properties of DSSC of 1.0%wt. CuO/TiO_2 electrode sintered at 400°C for 2 hours 500 coats (N719 dye)

Number of cell	V_{oc} (Volt)	J_{sc} (mA/cm^2)	Fill Factor	Efficiency (%)
1	0.66	2.20	0.59	0.86
2	0.66	2.14	0.60	0.85
3	0.68	2.06	0.54	0.75
4	0.65	2.17	0.64	0.90
5	0.69	2.47	0.71	1.21
Average	0.67	2.21	0.62	0.91±0.17

Table F.10 Electrochemical properties of DSSC of 3.0%wt. CuO/TiO_2 electrode sintered at 400°C for 2 hours 500 coats (N719 dye)

Number of cell	V_{oc} (Volt)	J_{sc} (mA/cm^2)	Fill Factor	Efficiency (%)
1	0.64	2.46	0.75	1.18
2	0.61	2.32	0.63	0.90
3	0.60	2.04	0.69	0.84

Number of cell	V_{oc} (Volt)	J_{sc} (mA/cm^2)	Fill Factor	Efficiency (%)
4	0.64	2.27	0.56	0.81
5	0.66	2.33	0.59	0.91
Average	0.63	2.29	0.64	0.93±0.15

Table F.11 Electrochemical properties of DSSC of 0.1%wt. NiO/TiO_2 electrode sintered at 400°C for 2 hours 500 coats

Number of cell	V_{oc} (Volt)	J_{sc} (mA/cm^2)	Fill Factor	Efficiency (%)
1	0.65	7.65	0.67	3.31
2	0.66	8.85	0.65	3.80
3	0.66	8.11	0.57	3.04
4	0.65	8.17	0.85	4.55
5	0.65	8.06	0.90	4.72
Average	0.65	8.17	0.73	3.88±0.74

Table F.12 Electrochemical properties of DSSC of 0.5%wt. NiO/TiO_2 electrode sintered at 400°C for 2 hours 500 coats

Number of cell	V_{oc} (Volt)	J_{sc} (mA/cm^2)	Fill Factor	Efficiency (%)
1	0.70	9.30	0.80	5.19
2	0.69	9.65	0.77	5.11
3	0.69	9.55	0.79	5.21
4	0.69	9.21	0.82	5.19
5	0.69	8.80	0.83	5.05
Average	0.69	9.30	0.80	5.15±0.07

Table F.13 Electrochemical properties of DSSC of 1.0%wt. NiO/TiO_2 electrode sintered at 400°C for 2 hours 500 coats

Number of cell	V_{oc} (Volt)	J_{sc} (mA/cm^2)	Fill Factor	Efficiency (%)
1	0.69	6.89	0.88	4.18
2	0.67	6.44	0.86	3.70
3	0.66	6.96	0.70	3.22
4	0.67	6.94	0.74	3.41
5	0.68	6.97	0.69	3.27
Average	0.67	6.84	0.77	3.55±0.40

Table F.14 Electrochemical properties of DSSC of 3.0%wt. NiO/TiO_2 electrode sintered at 400°C for 2 hours 500 coats

Number of cell	V_{oc} (Volt)	J_{sc} (mA/cm^2)	Fill Factor	Efficiency (%)
1	0.68	6.58	0.66	2.94
2	0.70	7.30	0.61	3.12
3	0.70	7.33	0.65	3.35
4	0.70	6.34	0.65	2.89
5	0.70	5.10	0.82	2.92
Average	0.69	6.53	0.69	3.04±0.19

Table F.15 Electrochemical properties of DSSC of 0.1%wt. In_2O_3/TiO_2 electrode sintered at 400°C for 2 hours 500 coats

Number of cell	V_{oc} (Volt)	J_{sc} (mA/cm^2)	Fill Factor	Efficiency (%)
1	0.66	5.98	0.75	2.98
2	0.66	6.59	0.63	2.77
3	0.66	6.49	0.64	2.74

Number of cell	V_{oc} (Volt)	J_{sc} (mA/cm^2)	Fill Factor	Efficiency (%)
4	0.68	6.51	0.64	2.82
5	0.67	6.50	0.65	2.80
Average	0.67	6.41	0.66	2.82±0.09

Table F.16 Electrochemical properties of DSSC of 0.5%wt. In_2O_3/TiO_2 electrode sintered at 400°C for 2 hours 500 coats

Number of cell	V_{oc} (Volt)	J_{sc} (mA/cm^2)	Fill Factor	Efficiency (%)
1	0.65	12.80	0.51	4.26
2	0.72	10.67	0.66	5.08
3	0.68	8.34	0.77	4.32
4	0.67	12.62	0.64	5.38
5	0.65	12.75	0.64	5.30
Average	0.67	11.44	0.64	4.87±0.54

Table F.17 Electrochemical properties of DSSC of 1.0%wt. In_2O_3/TiO_2 electrode sintered at 400°C for 2 hours 500 coats

Number of cell	V_{oc} (Volt)	J_{sc} (mA/cm^2)	Fill Factor	Efficiency (%)
1	0.70	12.70	0.81	7.27
2	0.72	10.67	0.66	5.08
3	0.69	9.81	0.84	5.65
4	0.69	12.94	0.70	6.26
5	0.69	11.99	0.81	6.77
Average	0.70	11.62	0.76	6.21±0.87

Table F.18 Electrochemical properties of DSSC of 3.0%wt. In_2O_3/TiO_2 electrode sintered at 400°C for 2 hours 500 coats

Number of cell	V_{oc} (Volt)	J_{sc} (mA/cm^2)	Fill Factor	Efficiency (%)
1	0.63	5.17	0.39	1.28
2	0.76	5.24	0.66	2.63
3	0.73	5.34	0.69	2.72
4	0.74	5.41	0.72	2.88
5	0.73	5.45	0.69	2.73
Average	0.72	5.32	0.63	2.45±0.66

Table F.19 Electrochemical properties of DSSC of double-layered electrode of pure TiO_2 (under-layer) sintered at 400°C for 2 hours 30 minutes 250 coats and 1.0%wt. In_2O_3/TiO_2 (over-layer) sintered at 400°C for 30 minutes 250 coats

Number of cell	V_{oc} (Volt)	J_{sc} (mA/cm^2)	Fill Factor	Efficiency (%)
1	0.701	14.05	0.84	8.29
2	0.714	13.76	0.80	7.88
3	0.644	13.26	0.88	7.47
4	0.695	13.47	0.82	7.70
5	0.683	14.03	0.88	8.43
Average	0.69	13.71	0.84	7.95±0.40

Table F.20 Electrochemical properties of DSSC of double-layered electrode of 1.0%wt. In_2O_3/TiO_2 (under-layer) sintered at 400°C for 2 hours 30 minutes 250 coats and pure TiO_2 (over-layer) sintered at 400°C for 30 minutes 250 coats

Number of cell	V_{oc} (Volt)	J_{sc} (mA/cm^2)	Fill Factor	Efficiency (%)
1	0.66	14.12	0.84	7.77
2	0.66	13.15	0.82	7.09
3	0.69	12.18	0.82	6.93
4	0.65	13.16	0.82	6.99
5	0.68	13.00	0.80	7.14
Average	0.67	13.12	0.82	7.18±0.34

VITA

Sakun Preedavijitkul was born on April 25, 1994 in Bangkok, Thailand. He finished high school from Protpittayapayat school, Thailand, and received the bachelor's degree of chemical engineering, King Mongkut's Institute of Technology Ladkrabang, in 2016. He continued his master degree in chemical engineering at Center of Excellence on Catalysis and Catalytic Reaction Engineering, Chulalongkorn University.

Sakun Preedavijitkul and Akawat Sirisuk. Improving the efficiency of dye-sensitized solar cells with spray-coated TiO2 electrode modified by CuO. Proceeding of pure and applied chemistry international conference, Prince of Songkla University, Hatyai, Songkhla, Thailand. Feb. 7-9, 2018 (PACCON2018)